Reply to the reviewers

Dear Editor,

Thank you for your comments and corrections. Please find below our reply in blue font, while reviewer's comments are in black font.

We also wish to thank the four referees for their very positive and constructive comments and for their hard work on our manuscript.

The manuscript has been significantly re-organized and changed according to suggestions and comments by the four referees.

Philippe Steer and co-authors

***

General comments:

I here summarized some significant comments that were common to several referees.

1) Technical corrections, specific comments and proofreading: Referee #1, Robert Sare and George Hilley

Most technical corrections pointed out by the referees were corrected. Note however, that we were unable to access the Hypothesis link given by George Hilley.

2) Paper organization is not optimal as some parts of the Results and Discussion should be switched: Referee #1. Moreover, Referee #1, Wolfgang Schwanghart and Robert Sare have pointed out that the paper is quite lengthy and that the writing could be more concise, in particular by moving minor sections in the appendix.

We agree with this comment and we have therefore reorganized the paper and tried to limit the length of the paper, which was difficult due to the numerous interesting comments made the four referees.

→ For clarity and readability issue, we have separated the Results section in four sections:

- 4 Magnitude, displacement and temporal distributions of earthquakes and co-seismic knickpoints
- 5 Knickpoints along single river profiles
- 6 Knickpoints along successive parallel rivers
- 7 Knickpoint detectability

The part about knickpoint detectability is kept as a result but is appears as the last result. The section on "Fault burial mechanism by intermittent sediment cover" is now part of the Results

→ To reduce (or to not increase) the length of the paper, we have:

- Decided to let Figure A1 in the appendice, despite the suggestion by Referee # 1 to include this Figure in Fig. 9. Indeed, if we agree that Figure A1 can help to understand Figure 9, Figure A1 is not a prerequisite to understand Figure 9.
- Moved some significant parts of the manuscript (including some figures) in the Appendices.
- Shorten some sentences to be more direct.
- Reduced the size of the figures (and of the description of the results) by considering only 2 end-member models instead of the 4 models described in the initial manuscript.

3) Erosion law: Wolfgang Schwanghart and Robert Sare
   Citing, for instance, Wolfgang Schwanghart: "However, you are raising interesting points in the discussion that you could actually pick up in your study. In particular the nonlinear stream power incision model with exponents unequal to one would be interesting to tackle. Why? Because, if n>1 then knickpoints with larger step heights would travel faster, and potentially coalesce with smaller ones. Now if that is the case, then traces of smaller earthquakes are obliterated by larger ones. This would have severe implications for the inference of fault activity and earthquakes from knickpoints. I am not an expert in Lagrangian numerical models and meshfree simulations, but I guess that the nonlinear model should not be too hard to implement."

We agree with this comment that implementing a non-linear dependency to slope for the stream power law in a Lagrangian framework is relatively straightforward. However, the main issue is that in this paper we are considering vertical knickpoints, which have by definition an infinite slope. This is not an issue for a linear model, as the slope exponent is n-1=0 (rather than n=1 in the Eulerian framework): $\frac{dy}{dt} = KA^m S^{n-1}$, which is by itself a nice outcome of Lagrangian models. However, for a value of n different than one (i.e. for non-linear models), there is no solution to this equation for infinite slopes. Moreover, we are not confident that larger knickpoints would migrate faster or slower in a non-linear model, for a constant slope.

Yet, the issue of the role of knickpoint height on migration rates is an idea, suggested by empirical (Baynes, personal communcation) and theoretical results, (Scheingross and Lamb, 2017) that deserved to be explored.

→ Therefore, we have added a section in the Results (section 5.2) and a figure (Fig. 7) to explore the role of a dependency of knickpoint retreat rate to their height on river profile development and on knickpoint height distribution.

Response to comments by Referee #1:

We thank Referee #1 for his work on this manuscript, his positive appreciation and for his many advices.

Landscape evolution models (LEMs) are in most cases driven by simplistic boundary conditions. Rock uplift (or translation in the case of strike-slip) due to fault motion may change through time, but is generally treated as a time-averaged rate, and the effects of individual uplift events at the earthquake scale are generally not considered. Yet there is a growing sense in our community that rivers may be valuable indicators of paleoseismic activity, and potentially current seismic hazards. In this contribution, Steer et al make a well-considered and important step towards a better understanding of how rivers respond to sequences of earthquakes. The authors present a simple model for how earthquakes shape river profiles under idealized conditions (i.e., under the assumption that knickpoints propagate unchanged upstream at a constant velocity). They use the model to make several tests of resulting river profile form, including exploring the effects of 1) the variance of the normal distribution of earthquake depths, 2) along-fault distance of a set of parallel rivers, and 3) various sediment cover scenarios.

The authors make several interesting findings. They find that incorporating both seismic and aseismic slip leads to only larger earthquakes being expressed in the river profile. They find that the degree of seismic coupling (seismic vs aseismic slip) also yields diagnostic changes in profile form. They assess the appropriateness of modern DEMs for extracting knickpoints in different seismic situations, and suggest that in fully coupled faults DEM resolution would have to be unreasonably high to extract knickpoints associated with individual earthquakes. They find a length scale above which correlation between the profiles of parallel rivers along the fault should no longer be expected due to the limited reach of a given earthquake along the fault plane. Finally, they identify situations in which sediment cover dynamics dominate seismically induced knickpoints and vice versa.

GENERAL COMMENTS

I really enjoyed this paper. The study is very novel in considering how the specifics of seismicity are expressed in the river profile. It is also timely as it affects both landscape evolution modelling and the inversion of river profiles obtained from high resolution DEMs. I find the study to be well thought out and well executed, and very appropriate for ESurf. My recommendation is to publish after minor revisions, which have very little to do with changing the science and mostly deal with the presentation.

I have four main comments:

1) Explanations of key terms and variables in the seismic modelling portions of the manuscript could be improved. I am a surface processes person, so it may be that I am exceptionally deficient in this department. However, since this paper is submitted to ESurf, I doubt that I am alone in wishing for clearer explanations in the sections dealing with seismic modelling. For example, the concepts of aseismic and interseismic deformation are not defined where they first occur on line 17 of page 2. I have marked in the specific comments other places where I think some easy additional explanations would help typical ESurf readers understand the paper.

→We now give definitions of some key terms associated to seismic modelling. We now define in the text: seismic slip, aseismic slip, seismic coupling etc.

2) These comments pertain to the organization of the manuscript. The results section is very clear for sections 4.1, 4.2, and 4.3. However, we then jump to "4.4 Knickpoint detectability," which is really not itself a result but an implication of the findings related to knickpoint height and spacing that the authors reported in Figure 6 and section 4.3. To me it seems that section 4.4 and Figure 7 belong in the discussion section. To be clear I think that this discussion of knickpoint detectability is great and should certainly remain in the paper, but since the authors don't actually do any detection of knickpoints in the paper it belongs in the discussion.

Figure 9 shows a very interesting (and important!) result, with major implications for studies using river profiles to infer seismic history. But Figure A1 is important to understanding Figure 9. I suggest that Figure A1 be combined with Figure 9 so that all of this information is in one place in the main text.

Much of section 5.5 describes and contains results of a set of model simulations addressing the role of sediment cover. These are again great, but it does not make sense to me to locate them in the discussion after such sections as "model limitations". Most of section 5.5, including figures 10 and 11, should be relocated to the results section, because these are really just the results of simulations. Any remaining text that does more than describe the results (e.g., the very helpful writing on lines 21-30 of page 23) can remain in the discussion.

We globally agree with this comment (except including Figure A1 inside Figure 9).

→ See response to General comment 2.

3) There are some places in the manuscript where awkward phrasing or sentence structure make reading difficult. I have marked many of these below in "technical corrections," but I would encourage one last thorough proofreading by the authors before resubmission.

Done.

→ See response to General comment 1.

4) I was excited to see that the model is available on Github. I ask the authors to consider associating the exact version of the model used for the paper with its own DOI and reporting that DOI in the code availability section. That way, if the model ever gets changed, interested readers can always find the version associated with this paper. This is easily done (10 minutes) with GitHub and Zenodo: https://guides.github.com/activities/citable-code/.

Excellent advice.

→ The DOI is 10.5281/zenodo.2654819 and we have added a reference: Steer and Croissant, 2019

Response to comments by Wolfgang Schwanghart:

We thank Wolfgang Schwanghart for his work on our manuscript and for his suggestion to use non-linear erosion laws.

Steer et al. analyse how seismic fault slip translates into the formation of knickpoints along fault-crossing rivers. Combining a stochastic model of earthquakes, earthquake ruptures, and seismic and aseismic slip with a deterministic model of river profile evolution, they present a number of interesting simulation results that can be readily tested in the field or with digital elevation models.

Major comments

(1) I really like the comprehensive review of the existing body of literature on knickpoints in river profiles. This is a very helpful resource for anyone who works on this topic. Yet, this entails that the manuscript is quite lengthy at times. I do not consider this as a significant weakness of the paper, however.

→ See response to General comment 1.

(2) The major part of the methods chapter is concerned with the seismic model. In comparison, the description of the fluvial model is rather terse. This imbalance is also reflected by the code that the authors make available on github. I think that this imbalance arises from the very simplistic treatment of fluvial processes. Please correct me if I am wrong, but isn't the profile just a linear transformation of cumulative slip along the fault? In other words: If knickpoint migration rate is constant in space, then the profile is a linearly scaled timeseries of cumulative slip. Now, constant knickpoint migration rates do make sense in this context, unless we are dealing with catchments of only a few square kilometers area. However, you are raising interesting points in the discussion that you could actually pick up in your study. In particular the nonlinear stream power incision model with exponents unequal to one would be interesting to tackle. Why? Because, if $n>1$ then knickpoints with larger step heights would travel faster, and potentially coalesce with smaller ones. Now if that is the case, then traces of smaller earthquakes are obliterated by larger ones. This would have severe implications for the inference of fault activity and earthquakes from knickpoints. I am not an expert in Lagrangian numerical models and meshfree simulations, but I guess that the nonlinear model should not be too hard to implement. Overall, I found the paper a very interesting read. It provides an excellent overview on knickpoint migration and offers an innovative approach to modelling the interaction between fault activity and the fluvial system. However, I think that there is likely a lot to be learnt if running the simulations with the nonlinear stream power incision model, too, and encourage the authors to implement this model.

→ See response to General comment 3.

Response to comments by Robert Sare:

We thank Robert Sare for his work on our manuscript, for his technical comments as well as his suggestion to reorganize some parts of the manuscript.

This submission combines a stochastic model of earthquake occurrence with a stream power landscape evolution model to study the spatial distribution and detectability of co-seismic knickpoints generated by a buried thrust fault. The authors explore the effects of seismic coupling, channel spacing, and exogenous sedimentation on knickpoint expression in isolated and neighboring channels. Among the most significant findings is that a fault with a large seismogenic area and limited aseismic slip may produce a similar number of channel-rupturing earthquakes at all magnitudes. They also identify a channel spacing beyond which parallel channel profiles are poorly correlated due to limited rupture extent, and quantify detection limits for knickpoint identification as a function of data resolution. The authors close with a discussion of the impacts of cyclic sedimentation on knickpoint preservation. Overall, it is a novel contribution and the methodology is reasonably well documented. I think the manuscript could be accepted after moderate revisions and editing for length and clarity.

We thank Robert Sare for his work and his comments on our manuscript.

SPECIFIC COMMENTS

MAJOR POINTS

1. In general, the writing could be made more concise. One easy change might be to expand the appendix with some of the details and background. I've tried to indicate sections I felt could be moved to the appendix in the minor points below.

Done.

→ See response to General comment 2.

2. A summary table of symbols used would make the study more accessible (included in main text or appendix). This is particularly important because some of the notation (χ) has conflicting uses in geomorphology (drainage-area-normalized channel length) and seismology (seismic coupling coefficient calculated as a ratio of velocities or moments). It would also help to clarify model parameters like σ not always found in physics-based earthquake cycle models, to aid comparison to something like the half width of the seismogenic zone in other studies.

We agree with this comment.

→ We have added a table of variable notation and definition in Appendice C (to keep the paper not too long).

3. A simple schematic figure would be helpful: either a map view of the model domain showing rupture extent and channel spacing, or a profile view of the channel and fault geometry, or both. This may be available in previous work by the authors, in which case a citation pointing to the model set up figure would be very helpful early in the text.

We agree with this comment.

→ We have added a simple schematic sketch (Figure 1) showing the fault extent, earthquake ruptures as well as a single river profile. For readability issue, it was difficult to display more than one river profile.

4. I believe the LEM described starting on page 10, line 20 is better described as a one dimensional model of the channel profile. Lateral transport in the y direction is not considered. Regarding this model, a non-linear stream power rule ($n \neq 1$) is worth including in this paper. What if higher slope knickpoints migrate faster than low slope knickpoints? I was surprised to see this discussed at length in Section 5.4 without a comparison of linear and non-linear model results.

→ See response to General comment 3.

5. The methods used in Section 4.4 should be clearly described in the opening paragraph. The analysis counts known co-seismic knickpoints in down-sampled river profiles rather than detecting knickpoints without prior information (which "detectability" might imply to some readers). This provides a useful baseline which should be emphasized early in this section's text. I appreciated the resolution testing summarized in the closing paragraph of this section.

→ We have added a sentence too explain what we refer to as knickpoint detectability (lines 10-12 page 22): "In the following, we consider that a knickpoint is detectable if its height is greater than the vertical precision of topographic data and if its distance to adjacent knickpoints is greater than the horizontal resolution of topographic data."

6. The results shown in Figures 10 and 11 are quite interesting and I hope they inspire future work. Could the authors determine something like the maximum detectable tectonic knickpoint height as a function of sedimentation rate and periodicity for tectonically active catchments whose climactic history is well understood? What about superimposing several earthquake cycles with climatically varying sedimentation?

We agree that these results are interesting. However, we initially conceived this part as a discussion opening for the paper rather than a detailed result section. The work suggested by Robert Sare is obviously interesting, but we believe it would also lead to a longer paper, which was clearly pointed out as a weakness of the paper by several referees. We also think that this issue probably deserves another more focused paper.

MINOR POINTS

1. To justify the Poisson process claim in Section 4.2, a best-fit exponential function and standard error value (or other measure of goodness of fit) could be provided for each of the distributions of inter-event times in Figure 4. It appears that the decay is not necessarily exponential for the most aseismic model (4a). It might be better to weaken this claim if the decay is not exponential in all cases.

We agree that the most aseismic model is not clearly exhibiting an exponential decay, but this simply results from the lack of events (20 earthquakes) to characterize the distribution. Fitting exponential distribution would only highlight the effect of the number of events, and therefore seems of limited interest.

→ We have added a sentence to explain this (Lines 2-3 page 14).

2. Figure 5 and parts of Section 4.3 could be moved to the appendix. It is important to justify the choice of VR, but this distracts from the central result in this section.

We agree with this comment.

→ See response to General comment 2.

3. Figure 8 and parts of Section 4.5 could be moved to the appendix as Fig. 9 + A1 and Section 4.5 include sufficient detail.

We disagree with this comment as we believe it is important for the readers to see by themselves the similarity of successive rivers along a single fault.

4. The model fault is a moderately dipping thrust fault, but the knickpoints are generated as vertical discontinuities. How might knickpoint detectability, preservation, and the profile cross-correlations change if the knickpoints have a finite initial slope or if knickpoints are displaced horizontally? This is addressed in Section 5.1, but it would be particularly interesting in the case of a non-linear stream power rule if knickpoint slopes vary.

→ See response to General comment 3.

5. The link to the GitHub repository is nice to see. For a more direct citation, it would be best to archive the current version of the code and provide a DOI through Zenodo (https://guides.github.com/activities/citable-code/).

Excellent advice.

→ The DOI is 10.5281/zenodo.2654819 and we have added a reference: Steer and Croissant, 2019

Response to comments by George Hilley:

We thank George Hilley for his numerous suggestions and insights on our manuscript. They have helped us to analyze with more depth the results of our model. Yet, we were not able to fully accounts for all the comments made by George Hilley, and we hope that the changes we have made to the manuscript answers at least partially to some of them.

Review of "Statistical modelling of co-seismic knickpoint formation and river response to fault slip" by Steer et al.

Summary:

This paper combines a stochastic model for releasing accrued moment (by earthquakes, aftershocks, and creep) with a geomorphic model to advect surface-rupturing offsets upstream at a constant velocity along channels. The modeled fault is a 30 dipping thrust fault slipping at 15 mm/yr. The upstream advection rate of offsets generated by earthquakes is set to 10 cm/yr. Using these parameters, the authors investigate the range of generated profile forms, with an eye towards detectability of knickpoints produced by seismogenic offsets and the role that creep plays in river profile development. This speaks to the utilization of the distribution of knickpoint heights as a paleoseismic tool, and the use of constant (or smoothly varying) uplift rate boundary conditions versus individual offset events in modeling river profiles.

Recommendation:

This paper presents an interesting new approach to addressing several important questions in tectonic geomorphology: 1) under what circumstances are profiles approximated by constant or smoothly varying uplift rate conditions versus individual earthquakes, 2) given data sampling and accuracy, under what conditions might river profiles resolve past earthquakes, 3) how does the distribution of surface rupture magnitudes affect the interpretation of knickpoints in river profiles, and 4) what role does creep play in generating the profile forms of rivers traversing faults. I think the work has the potential to provide clarity to many of these issues, at least to the extent that it could nicely frame these problems and lay out a path for future field and modeling studies. As written, the paper contains the seeds of this, but could be reorganized, recast, and extended to be more impactful in this regard. Below, I make several observations and suggestions that are aimed at this purpose. The authors may argue that these suggestions are outside of the scope of this work given their aims. Yet, I worry that in its current form, the paper may not garner the impact it deserves. These are issues of preference, and so I leave it to the authors and editor to decide on whether or not these suggestions are appropriate for the scope of this work. Nonetheless, at a minimum, the paper needs some efficiency improvements and clarifications, which together probably constitute MODERATE TO MAJOR REVISIONS.

General Comments:

1) I have to admit that I found Section 2 confusing and largely unnecessary. I think it is being used to motivate the model that has been developed. But, an alternate approach would be to move directly from the Introduction to the Methods and use the literature cited to support the model selection. The discussion could then be used to cite and discuss literature that may complicate the model, and what impacts these studies might have on the fundamental results that are reported.

We disagree with this comment as most information given in this state-of-start section is required to introduce modelling strategies and model parameters that are given in the Methods section or later. More importantly, few (or no) papers have synthetized the literature about the links between earthquake activity, knickpoint formation and knickpoint propagation, and we embrace this opportunity in this paper.

2) I think the presentation of the model in Section 3 could be greatly simplified. It seems as though the following is done: 1) Earthquakes are drawn out of a G-R distribution whose patch sizes and offsets are determined by the Leonard scaling relations (aftershocks are then generated using BASS). 2) The hypocenters of the patches are located according to a Gaussian depth-distribution centered at the midpoint of the model domain, and are uniformly sampled along strike. A uniform slip rate is maintained, such that aseismic creep takes up what the earthquakes do not. 3) From these, surface-rupturing patches are identified, used to uplift surface channel points, and then the profile is advected horizontally at a prescribed rate. I'm not sure there is a need to bring the power-law incision model into this, since it is not really used, to the extent that the advection velocity is assumed constant.

We partially agree with this comment.

→ Following this comment, we do not root anymore the theory of our modelling approach in the stream power model and we have therefore removed the stream power law form the Methods section. Instead, we now discuss in Appendice A the relationship between the kinematic model and the stream power law.

→ However, we do not wish to over-simplify the description of the Methods as 1) some details of the methods are required to make the paper self-contained when there is no supporting literature and 2) the methods in itself is novel (at least in the Geomorphology community) and deserves to be precisely described as we hope it could be used in future studies or in other models.

3) I appreciate the comments of the reviewers with regard to examining more flexible geomorphic incision rules. I think that these criticisms are rooted in the fact that the paper is cast in terms of the power-law incision model. As mentioned in (2), the incision model is not really being used here anyway, at least not in any explicit way – the perturbations in the profile are simply being advected headward at a constant velocity. Thus, I would suggest taking the approach that you are using a zeroth-order geomorphic model of constant advection rate to match the simplicity of the offset model (see below for suggestions on this). These limitations can then be discussed in the Discussion, and a path toward future work can be laid out. This avoids issues related to geomorphic model selection, since you would simply be using a kinematically prescribed description of knickpoint creation and migration. The appropriateness of this simplified model could then be discussed later in the paper and put into the context of the incision rule.

See responses to previous comment 2) and to General comment 3

4) It seems that with a little more thinking, the spirit of this work could go a long way in clarifying the role that individual earthquakes play in producing channel profiles. First, I think that the dimensionality of the problem could be reduced and the results could be clarified. The current study uses a single slip

rate, which is implemented through events created by the G-R relations, and completed by creep to advect these knickpoints at a velocity, Vr, which is either constant or randomly sampled. It seems as though the profile geometry will be approximated by uniform uplift rate when the spacing between successive knickpionts is small, and will be detectable as individual offset events when this distance is large. This suggests a horizontal length-scale L that varies with Vr * t, where t is the recurrence time of some earthquake. Additionally, the vertical dimension of the model might be normalized by the vertical displacement (d) that occurs during this earthquake. Normalized time in this case would simply reflect the number of earthquakes that have occurred and the fraction of the earthquake cycle that has been experienced. Given this parameterization, if one starts with the simple case of a time-predictable characteristic earthquake, the two length scales can be related through the slip rate along the fault as t = d / (Vs sin(dip)), meaning that L = d (Vr / Vs) / sin(dip). The extremes of this length scale should revert to the single-event, and constant uplift rate cases as t* becomes large.

I understand that this is not what the current study has done, as it is a stochastic model that is used here. But, I wonder if it would be more illustrative to restructure the paper to start with a simple toy model that demonstrates this point. Beginning with a characteristic earthquake that ruptures the surface in this way, one could use the procedure for uplifting and advecting the surface profile in normalized space (x* = x / L; z* = z / d). You could show, in normalized coordinates, that this is just a unity increment in z* with each unity increment in x* at the beginning of each earthquake cycle. When you do this when t* is large, for a range of x* between 0-5, you'll see the earthquakes, when x* is between 0-500, you'll see a constant slope (more-or-less). I think that these are the two end-members that are being sought. Since the uniform uplift case will produce a slope of one in this space, you could even use the deviation from this line as a measure of how far / close to the uniform condition you are. You could then define a horizontal length-scale that defines the "detection limit" that one might expect to observe in the field, and cast this in terms of the multiple of L at which individual earthquakes bleed into continuous uplift to see those d*(Vr/Vs)/sin(dip) conditions for which one might expect to be able to see individual events clearly.

After this simple exercise is completed, then the stochastic model would be a nice extension of the basic idea. In this case, the productivity rates of the a-value of GR could be cast in terms of the seismogenic fault slip rates, and this could be used with the maximum magnitude event to define recurrence time, which could serve as the normalizing time-scale. Experiments could be performed, results normalized, etc. to examine the impact of the stochasticity on the character and range of knickpoints generated by such an exercise. Finally, W could then be varied in a way that creep could be added into the analysis, with its impact on the profile form (and knick point detectability) analyzed.

Such an incremental and non-dimensional casting of the problem might help to distill the problem to its essence for illustration, show how increasing realism in the way in which seismic moment is released impacts the profile forms, and broaden the applicability of the analysis to a wide range of fault geometry and slip rate conditions through the non-dimensionalization. The discussion could then be focussed on: 1) How Vr might actually relate to the power-law incision model (since the analysis can be understood without the context of the incision rule), 2) What the impacts of more complicated variations of Vr with things like channel slope might be (i.e., n = 1), 3) what lithologic / climatic conditions might be appropriate for archiving meaningful paleoseismology information (ranges in K for different watershed areas that produce Vr/Vs ratios that yield detectable knickpoints), 4) what the impact of heterogeneities in lithologies and transport processes (e.g., transport-limited alluvial conditions) might be on profile form and detectability, and 5) other model limitations.

We appreciate this comment that is very insightful. Yet, we are not convinced that extending our modelling approach to- or normalizing our result by- a time-predictable model is relevant.

First, the notion of time-predictable earthquake was popular in the 80's due to its simplicity and apparent quality to reproduce some paleo-seismological records. However, time-predictable models are generally not considered anymore when modelling more resolute paleo-seismological records or to infer seismic hazards (which are the two common disciplines that use statistical models to investigate spatio-temporal series of earthquakes), and most study now consider mechanical-based model or ETAS. Moreover, time-predictable models are already very routinely used in landscape evolution models (and yet most model developers do not conscientiously know it) that generally consider a constant time-step and uplift rate with a sharp boundary condition, which directly translates into a time-predictable model of block uplift.

Second, the link between a time-predictable earthquake model and the stochastic model we use is difficult to establish because:

1) The notion of characteristic recurrence time is fundamental for a time-predictable earthquake model but has no obvious mathematical meaning in a stochastic model as there is no characteristic magnitude. Recurrence time is generally defined as the (mean) time separating successive events of magnitude above a defined threshold. In the purely seismic model, considering a magnitude threshold of 7 or 7.3 (which is the maximum magnitude allowed using the fault dimension of our model) leads to significatively different mean recurrence time of 240 years (min=3, max=1400 years) or 700 years (min=3, max=2340 years), while the minimum height of the knickpoints formed by these magnitudes, 1.25 or 1.7 m, is similar. Normalizing time (or knickpoint height and horizontal distance) by these two recurrence times (or by the recurrence time multiplied by knickpoint or fault velocity) would lead to very different results.
2) The height distribution of knickpoint has no dependency over fault slip rate. Indeed, increasing fault slip rate will only increases earthquake frequency without changing the distribution or range of earthquake magnitudes. Only a change in fault dimension will result in a change in the upper bound of the range of modelled earthquake magnitudes.

However, we agree that the section on "Knickpoint detectability" could have been described with a less model-dependent formalism. Following this comment, we now assess knickpoint detectability using a range of fault slip rate Vf and knickpoint retreat rate Vr. Indeed, the ratio Vf/Vr, that is a dimensionless number that directly represents the river slope, also conditions the detectability of knickpoints: 1) Increasing Vf increases the frequency of knickpoint formation and decreases the horizontal spacing between successive knickpoints; 2) Increasing Vr increases the spacing between successive knickpoints. With this new analysis, we can now predict (under the model limitations) what would be the detectability of knickpoints along any bedrock river, colluvial channel or hillslope with only requiring knowledge of its slope. As the slope of a channel or hillslope is relatively easy to obtain, this clearly represents a result with potentially large implications.

→ We have therefore deeply modified the section on knickpoint detectability (section 7) and the associated figure (Fig. 12) to account for these modifications.

5) I was not altogether clear on how the horizontal motions produced by the 30 dipping thrust fault were actually treated in the knick point evolution model. I think that the authors are probably resolving the component of slip into the vertical direction, and advecting this offset upstream. This creates two related issues. First, the horizontal motions produced by fault slip will act in an opposing direction to the knickpoint migration, and so some adjustment to Vr needs to be made to account for this. Given Vr and Vs used in the base-case simulation, this will not be a large contributor to the net advection velocity, yet it will constitute punctuated motion during offset events (or constant during creep). Nonetheless, as Vr approaches the 1mm/yr end-member shown in Figure 5, this effect will be

important. Related to this, it is worth some text in the discussion that, if the location at which offsets are generated remains fixed, this assumes that the constant-elevation boundary condition is not advected by the horizontal motions. While this is likely the case in many circumstances, I'm not sure it can be regarded as universally true. Advance of the hanging wall of thrusts over the topographic surface in a ramp-flat geometry requires motion of the boundary condition. This will probably happen when Vr - Vs cos(dip) produces a negative value. In these cases, knickpoints will be created and will advance into the hanging wall, but the coordinate system needs to move toward the footwall at this velocity. As the thrust sheet advances over the topography, the ramp-flat geometry might cause motions to parallel to the topographic surface, and so discrete vertical offsets may not exist in these situations as a fault-bend fold develops at the ramp-flat transition. I'm not advocating that the authors implement this, as it is clearly beyond the scope of this work. But, it is an opportunity to frame future studies in the Discussion, which might track down some of these issues.

The model we have developed does not consider knickpoint advection during fault motion. Moreover, we have simplified our model by imposing that all motion on the fault act in the vertical direction, neglecting the role of the dip angle of the fault.

→ Following this comment, we now discuss in section 8.3 (page 2.5) the influence of horizontal tectonic displacements on our results.

6) In the spirit of matching the complexity of models to one another, I wonder if the inclusion of aftershocks in the earthquake model creates a mismatch to the constant advection-velocity geomorphic model. Indeed, I might argue that the appropriate match to the complexity of the geomorphic model that is used would be a time-predictable characteristic earthquake offset. But, I think there is real value in extending the model to creating events according to a G-R distribution. Analyzing the effect of creep also seems important. What was not completely clear was how much of a difference the aftershock component of the model makes in the end analysis. Could it be eliminated without loss of insight? I am not saying that this is the case, but the process by which the authors build the study – that all of the complexity is introduced at the same time rather than an incremental inclusion of effects to assess each's importance – makes this difficult to determine.

We agree with this comment. Indeed, aftershocks play a secondary role in terms of river uplift or knickpoint formation, while they require a relatively high-level of complexity for their implementation in the model compared to mainshock modelling (i.e. that simply follows the Gutenberg-Richter law).

→ We now discuss the role of mainshocks and aftershocks in section 8.4 of the Discussion.

Specific Comments:

I started marking up the PDF in Hypothes.is. Given that the paper may need some restructuring (if the authors find any of the above commentary valuable), I tapered off the detailed editing after Section 2.

https://hyp.is/go?url=urn%3Ax-pdf%3Ace60be1c82ce3c4e151f9f5839f60e0c

→ We were unfortunately unable to access this link that redirected us to an URL error.

Summary:

I hope that the authors find these comments helpful in preparing their revision. Again, I think that this work has the potential to provide clarity as to when, and under what conditions individual offsets may be resolved within the profile of channels. It also has the opportunity to frame many future modeling and field studies focused on tracking down and field-testing some of the assumptions made in the approach. In this regard, I hope that the authors understand that my comments are aimed at seeing that the work ultimately has the impact that it deserves.

We have tried to enhance the quality of our paper regarding these insightful comments. We hope we have at least partially succeeded in convincing the referee of this.

Statistical modelling of co-seismic knickpoint formation and river response to fault slip

Philippe Steer[1], Thomas Croissant[1,a], Edwin Baynes[1,b], Dimitri Lague[1]
[1]Univ Rennes, CNRS, Géosciences Rennes - UMR 6118, F-35000 Rennes, France.
[a]now at Department of Geography, Durham University, Durham, UK.
[b]now at Department of Civil and Environmental Engineering, University of Auckland, Auckland, New Zealand

Correspondence to: Philippe Steer (philippe.steer@univ-rennes1.fr)

Abstract. Most landscape evolution models adopt the paradigm of constant and uniform uplift. It results that the role of fault activity and earthquakes on landscape building is understood under simplistic boundary conditions. Here, we develop a numerical model to investigate river profile development subjected to fault displacement by earthquakes and erosion. The model generates earthquakes, including mainshocks and aftershocks, that respect the classical scaling laws observed for earthquakes. The distribution of seismic and aseismic slip can be partitioned following a spatial distribution of mainshocks along the fault plane. Slope patches, such as knickpoints, induced by fault slip are then migrated at a constant rate upstream a river crossing the fault. A major result is that this new model ~~produces co-seismic knickpoints with~~predicts a uniform ~~height~~ distribution of earthquake magnitude rupturing a river that crosses a fault trace and in turn a negative exponential distribution of knickpoint height for a fully coupled fault, i.e. with only co-seismic slip. Increasing aseismic slip at shallow depths, and decreasing shallow seismicity, censors the ~~range~~ magnitude range of earthquakes cutting the river towards large magnitudes and leads to less frequent but higher amplitude knickpoints, on average. Inter-knickpoint distance or time between successive knickpoints follows an exponential decay law.

Using classical rates for fault slip, 15 mm.yr^{-1} and knickpoint retreat, 0.1 m.yr^{-1}, leads to high spatial densities of knickpoints ~~requiring sub-metric spatial resolution to distinguish them.~~. We find that knickpoint detectability, relatively to the resolution of topographic data, decreases with river slope that is equal to the ratio between fault slip rate and knickpoint retreat rate. Vertical detectability is only defined by the precision of the topographic data that sets the lower magnitude leading to a discernible offset. Considering a retreat rate with a dependency on knickpoint height leads to the merging of small knickpoints into larger one and larger than the maximum offset produced by individual earthquakes. Moreover~~The correlation between the topographic profiles of successive parallel rivers cutting the fault remains positive for distance along the fault of less than half the maximum earthquake rupture length. This suggests that river topography can be used for paleo-seismological analysis and to assess fault slip partitioning between aseismic and seismic slip. Yet~~, considering simple scenarios of fault burial by intermittent sediment cover, driven by climatic changes or linked to earthquake occurrence, leads to knickpoint distributions and river profiles markedly different from the case with no sediment cover. This highlights the potential role of sediments in modulating and potentially altering the expression of tectonic activity in river profiles and surface topography. The correlation

between the topographic profiles of successive parallel rivers cutting the fault remains positive for distance along the fault of less than half the maximum earthquake rupture length. This suggests that river topography can be used for paleo-seismological analysis and to assess fault slip partitioning between aseismic and seismic slip.

Last, the developed model can be coupled to more sophisticated landscape evolution models to investigate the role of earthquakes on landscape dynamics.

1 Introduction

The interactions ~~between~~among tectonics, climate and surface processes govern the evolution of the Earth's topography (e.g. Willet et al., 1999; Whipple, 2009). Among the potential link and feedbacks between tectonics and surface processes, the building of topographic slopes by tectonic deformation is critical. Erosion rates and most geomorphological processes are strongly sensitive to local slope, including river incision (e.g. Whipple and Tucker, 1999), glacial carving (e.g. Herman and Braun, 2008), soil creep (e.g. McKean et al., 1993) and hillslope mass wasting (e.g. Keefer, 1994). The dependency to slope can be linear or non-linear, mainly due to threshold effects or to a power-law behaviour. For instance, a theoretical model combined with a data compilation suggests that river incision rate is linearly dependent on slope at knickpoints, and more than linearly dependent on slope for more gentle stream profiles (Lague, 2014). This is pivotal, as temporal variations in tectonic displacement and in slope building cannot be averaged out when considering river profile evolution using an erosion law with a non-linear dependency to slope. In addition to slope, the height of knickpoints (i.e. with a slope above average local slope) and waterfalls (i.e. with a slope close to infinity) appears as a fundamental ingredient of their survival, retreat rate and river incision (Hayakawa and Matsukura, 2003; Baynes et al., 2015; Scheingross and Lamb, 2017). Similar issues arise for hillslope dynamics impacted by fault scarp development (Arrowsmith et al., 1996) and possibly for faults in glaciated landscapes. Despite this, most landscape evolution models of topographic growth consider slope building as a continuous process resulting from a constant (or smoothly varying) uplift rate (e.g. Braun and Willett, 2013; Thieulot et al., 2014; Campforts et al., 2017). There is therefore a clear need to define how tectonic deformation ~~build~~builds topographic slopes in numerical models.

The expression of tectonic deformation on topographic slope is diverse, and its spatial and temporal scales range from meters to continents and from instantaneous to geological times, respectively. Tectonic deformation can 1) instantaneously generate steep-to-infinite slopes when earthquakes rupture the Earth's surface (e.g. Wells and Coppersmith, 1994); 2) induce progressive slope building at the orogen scale and over a seismic cycle by aseismic deformation (i.e. deformation not associated to earthquakes) and interseimic deformation (i.e. deformation occurring in-between large magnitude earthquakes) (e.g. Cattin and Avouac, 2000) or by the deformation associated to earthquakes with no surface rupture; and 3) lead to longer-term topographic tilting at the orogen-to-continental-scale by isostatic readjustment (e.g. Watts, 2001) or viscous ~~mantellic~~mantle flow (e.g. Braun, 2010). In this paper, we focus on the building of topographic slopes by fault slip at the ~~intersect~~intersection between a fault trace and a river. This is motivated first by the fact that the greatest slopes are expected to occur by faulting, and second by the already well understood role of isostasy and viscous deformation on topography (e.g. Watts, 2001; Braun, 2010). In active mountain belts, displacement along frontal thrust faults can lead to the development of co-seismic waterfalls, knickpoints and knickzones than can reach several meters of elevation (e.g. Boulton and Whittaker, 2009; Yanites et al., 2010; Cook et al., 2013). These differential topographies, associated to high slopes, are referred to as slope patches in the following work. These slope patches have long been recognized as potential markers of the dynamic response of rivers (e.g. Gilbert, 1896) to transient conditions, not limited to changes in tectonic activity, and including base level fall and lithological contrasts, among others. Yet, in active tectonic areas, knickpoints are frequently associated to fault activity and transience in uplift rate (e.g. van der Beek et al., 2001; Quigley et al., 2006; Dorsey and Roering, 2006; Yildirim et al., 2011). These slope patches generated by frontal thrusts along a river migrate upstream by erosion and are expected to set the erosion rate of the entire landscape (Rosenbloom and Anderson, 1994; Royden and Perron, 2013; Yanites et al., 2010; Cook et al., 2013).

Fault slip and surface rupture classically occur by seismic slip during earthquakes. However, associating individual earthquakes to knickpoints, or associating series of knickpoints to series of earthquakes remains challenging from field data. We therefore use in this paper a statistical model of earthquakes to simulate the expected slope and height distributions of the slope patches generated by earthquakes (i.e. fault seismic slip) and fault aseismic slip at the ~~intersect~~intersection between a thrust fault and a river. This model uses the branching aftershock sequence (BASS) model (Turcotte et al., 2007) to simulate temporal and spatial series of earthquakes~~. Their rupture extents and displacements~~ based on the main statistical and scaling laws of earthquakes. The rupture extent and displacement of earthquakes are inferred using classical scaling laws (Leonard, 2010). We focus on the response of rivers and analyse the resulting knickpoint height distribution and their migration distance along a single river, in near-fault conditions. We also infer the correlation between the topography of successive parallel rivers distributed along the strike of a single fault. The obtained results are then discussed with regards to the potential of knickpoints and waterfalls to offer paleo-seismological constraints, and to the necessity of considering time-variable uplift accounting for earthquake sequences in landscape evolution models. It is important to stress out that this study does not aim to investigate specific geomorphological settings, but to give general theoretical and modelling arguments to the interpretation of river profiles upstream of active faults.

2 State of the art: linking fault slip to knickpoint formation and migration

2.1 From fault slip and earthquakes to surface ruptures and knickpoints

In near fault conditions, too few data characterizing fault rupture geometry at one location (e.g. along a river) exist to assess the distribution of the slope and height of surface ruptures resulting from earthquakes by local fault activity (e.g. Ewiak et al., 2015; Wei et al., 2015; Sun et al., 2016). Regional or global compilation of fault rupture by earthquakes (e.g. Wells and Coppersmith, 1994; Leonard, 2010; Boncio et al., 2018) offer another approach, that yet suffers from inescapable statistical biases mainly due to the use of faults with different slip rates, dimensions, seismogenic properties and records of paleo-earthquakes. In addition, small earthquakes associated with small rupture extents and co-seismic displacement are less likely to be identified in the field. For instance, using seismological scaling laws (Leonard, 2010), an earthquake of magnitude 3 on a thrust fault has a rupture length of 188 m and an average displacement of 1.2 cm. This displacement is clearly below the precision of current digital elevation models or in any case hidden by the inherent topographic roughness. ~~At the watershed scale, bedrock river slope increases upstream and scales negatively with water discharge or drainage area (Flint, 1974). However, this observation corresponds to a fundamental prediction of the stream power incision models (Howard and Kerby, 1983; Howard, 1994; Whipple and Tucker, 1999; Lague, 2014), and does not a priori reflect gradients in tectonic uplift or in initial slope distribution (i.e. before upstream migration by erosion).~~

Statistical or theoretical inferences offer another means to associate fault activity and earthquakes to surface ruptures and knickpoints. Earthquakes tend to universally follow the Gutenberg-Richter frequency-magnitude distribution in Eq. (1):

$$\log_{10}\left(N(\geq Mw)\right) = a - bMw, \qquad (1)$$

where Mw is the magnitude, $N(\geq Mw)$ is the number of earthquakes with magnitudes greater or equal to ~~Mw, b~~Mw, b is the exponent of the tail (referred to as the b-value), generally observed to be close to 1 ($0.5<b<1.5$), and ~~a~~a characterizes earthquake productivity (Gutenberg and Richter, 1944). ~~The b-value is generally observed to be close to 1 ($0.5<b<1.5$).~~The definitions of all variables used in this paper are summarized in Table C1. Assuming self-similarity, a b-value of 1 can be interpreted as the result of the successive segmentation of larger earthquakes into smaller earthquakes (Aki, 1981; King, 1983) so that any point along a 2D fault plane, including the ~~intersect~~intersection between the fault trace and a river, displays a uniform probability to be ruptured by earthquakes of any magnitude. ~~Because fault displacement D during an earthquake scales with seismic moment (Wells and Coppersmith, 1994; Leonard, 2010), it results that the distributions of surface rupture height at one location along the fault trace should also follow a uniform frequency-size distribution.~~ This inference only stands if the distribution of earthquakes along the fault plane is uniform. However, fault slip can occur by seismic slip~~ (i.e. here limited to fast earthquakes),~~, but also by aseismic deformation, including interseismic creep, postseismic deformation and slow slip events (e.g. Scholz, 1998; Peng and Gomberg, 2010; Avouac, 2015). The relative spatial and temporal distribution of aseismic and seismic slip along a fault plane is variable and still poorly understood. Yet, experimental results and the depth distribution of earthquakes along subduction or intraplate thrust faults suggest that shallow depths (< 5 km) are favourable to frictional stability and in turn to aseismic slip (Scholz 1998). This probably censors the magnitude range of earthquakes rupturing the surface towards large magnitudes associated with rupture extent greater than this minimum seismogenic depth.

2.2 Knickpoint formation

The transformation of surface ruptures into knickpoints remains a relatively enigmatic issue. Linking knickpoints to individual earthquakes is challenging, although some recently formed knickpoints have been clearly identified as the result from the surface rupture of a single large earthquake (e.g. Yanites et al., 2010; Cook et al., 2013). The transformation of individual surface ruptures into individual co-seismic knickpoints is not necessarily a bijective function and is more likely to be a surjective function. In other words, a knickpoint can be made of several surface ruptures. Indeed, if the time interval between two (or more) successive ruptures at the same location is less than a characteristic migration time required to segregate their topographic expressions, then the formed knickpoint will result from this succession of surface ruptures and earthquakes. An end-member setting favouring this behaviour is the case of fault scarps developing on hillslopes, which degradation is generally assumed to follow a diffusion law (e.g. Nash, 1980; Avouac, 1993; Arrowsmith et al., 1996; Roering et al., 1999; Tucker and Bradley, 2010). Moreover, in the downstream part of rivers, fault scarps can remain buried under a sediment cover due, for instance, to the development of an alluvial fan (Finnegan and Balco, 2013; Malatesta and Lamb, 2018). Development of the fault scarp height by successive ruptures ~~or a large one~~ or the thinning of the alluvial cover can then expose the scarp, in turn potentially forming a knickpoint that can erode and migrate. This intermittent fault burial mechanism can therefore produce knickpoints formed by the surface rupture of several earthquakes.

The burial of the fault during successions of aggradation-incision phases of an alluvial fan located immediately downstream of the fault (e.g. Carretier and Lucazeau, 2005) has not been considered in previous landscape evolution models. This mechanism is suggested to be a primary control of knickpoints and waterfalls formation by allowing the merging of several small co-seismic scarps formed during burial phases into single high-elevation waterfalls that migrate during latter incision phases (Finnegan and Balco, 2013; Malatesta and Lamb, 2018).

2.3 Knickpoint migration and preservation

Once formed, knickpoints can migrate upstream due to river erosion. Over geological time-scales (> 10^3 yr), rates of knickpoint retreat for bedrock rivers typically range between ~10^{-3} and ~10^{-1} m.yr^{-1} (e.g. Van Heijst and Postma, 2001). This range is also consistent with the order of magnitude of documented knickpoint retreat rates in Eastern Scotland (Bishop et al., 2005; Jansen et al., 2011), around ~10^{-1} m.yr^{-1}, in the Central Apennines, Italy and in the Hatay Graben, Southern Turkey (Whittaker and Boulton, 2012), between ~10^{-3} and ~10^{-2} m.yr^{-1}. However, on shorter time scales, significantly higher rates can be found with values potentially reaching ~10^0 or even ~10^1 m.yr^{-1}. For instance, the Niagara Falls retreated at a rate of a few meters per year over tens of years (Gilbert, 1907) and some knickpoints formed by the 1999 Chi-Chi earthquake in Taiwan even retreated by a few hundreds of meters over about ten years (Yanites et al., 2010; Cook et al., 2013). A more extensive analysis of the range of knickpoint retreat rates in relation to the observation time-scale can be found in Van Heijst and Postma (2001) and in Loget and Van Den Driessche (2009).

In detachment-limited conditions, the stream power incision model predicts that knickpoint horizontal migration or retreat follows a linear or non-linear kinematic wave in the upstream direction, depending on the slope exponent (e.g. Rosenbloom and Anderson, 1994; Tucker and Whipple, 2002; Whittaker and Boulton, 2012; Royden and Perron, 2013). This prediction is supported by the apparent correlation between retreat rate and drainage area or water discharge, deduced from field observation and experimental studies (Parker, 1977; Schumm et al., 1987; Rosenbloom and Anderson, 1994; Bishop et al., 2005; Crosby and Whipple, 2006; Loget et al., 2006; Berlin and Anderson, 2007). However, some experimental results show no dependency of retreat rate on water discharge, (Holland and Pickup, 1976), possibly due to the self-regulatory response of river geometry to water discharge through change in river channel width (Baynes et al., 2018). Other factors influencing retreat rate include, among others, sediment discharge (e.g. Jansen et al., 2011; Cook et al., 2013), flood events (e.g. Baynes et al., 2015), rock strength (e.g Stock and Montgomery, 1999; Hayakawa and Matsukura, 2003; Baynes et al., 2018), fracture density and orientation (Anton et al., 2015; Brocard et al., 2016) and the spacing and height of the waterfalls (Scheingross and Lamb, 2017).

Preservation of knickpoint shape during retreat is poorly understood as very little data exist on the temporal evolution of their shape. For instance, knickpoints along the Atacama Fault System are systematically reduced in height compared to the height of ruptures directly on the fault scarp (Ewiak et al., 2015). At the opposite, ten years after Chi-Chi earthquake, the height of co-seismic knickpoints was ranging from 1 to 18 m (Yanites et al., 2010), while the initial surface rupture was limited to 0.5 to 8 m in height (Chen et al., 2001). Theoretically, only the stream power model with a linear dependency on slope predicts the preservation of knickpoint shape, favoured by a parallel retreat (e.g. Rosenbloom and Anderson, 1994; Tucker and Whipple, 2002; Royden and Perron, 2013). A less than linear dependency on slope leads to concave knickpoints, while a more than linear dependency on slope leads to convex knickpoints. Transport-limited models, that reduce to advection-diffusion laws, lead to a diffusion of the differential topography associated to knickpoints. However, transport-limited models are likely more pertinent to predict the evolution of fault scarps along hillslopes (e.g. Rosenbloom and Anderson, 1994; Arrowsmith et al., 1996; Arrowsmith et al., 1998; Tucker and Whipple, 2002), and ~~evidences point towards~~evidence points toward a linear dependency on slope for knickpoint erosion (Lague, 2014). Yet, the transformation of fault activity and slip during earthquakes to knickpoints and hillslope scarps and their preservation throughout their subsequent erosion and retreat remains a challenging issue.

3 Methods~~: description of the numerical model~~

3.1 Fault setting

The tectonic setting considered here is the one of a typical active intracontinental thrust fault, able to generate earthquakes up to magnitude 7.3. The thrust fault has a length $L = 200$ km, a width $W = 30$ km, and a dip angle $\theta = 30°$ so that the fault tip is located at 15 km of depth. The duration of the simulation T is set to 10 kyr to cover many seismic cycles and for earthquakes to be well distributed along the finite fault plane~~ (Fig.~~. A schematic sketch illustrates the model setup (Fig. 1).

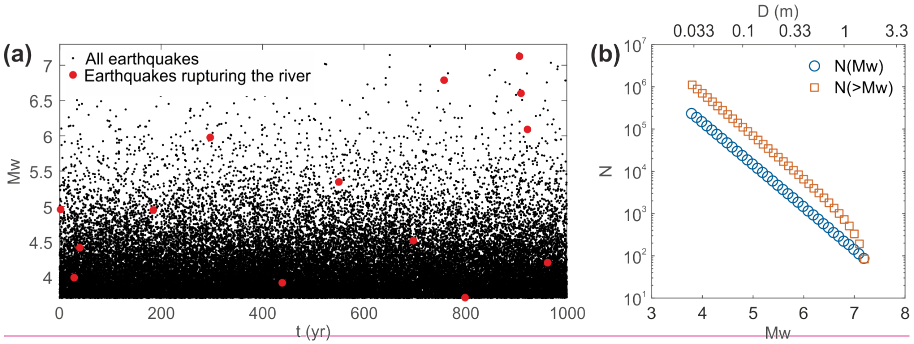

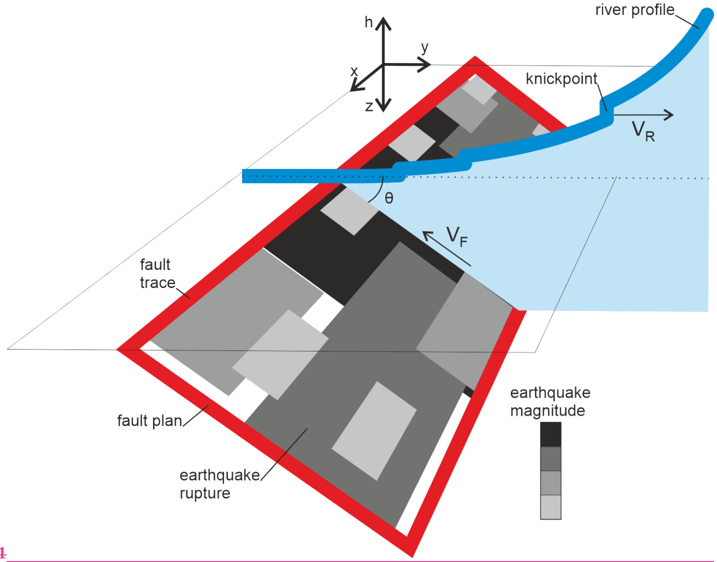

~~Figure 1~~

Figure 1. Schematic sketch showing the model setup. The fault plan, dipping with an angle θ, is represented by a red contour and includes the earthquakes and their ruptures represented by gray box, which color indicates the magnitude. The fault trace is aligned along the x-axis and earthquakes occur at depth z. The river profile is indicated by a blue line along the y-axis and has an elevation h. The river contains several knickpoints. Note that in this paper we only focus on knickpoints occurring in near-fault condition. The rate of fault slip is V_F while knickpoint migrate at a constant velocity V_R.

~~. Modeled seismicity and its statistical characteristics. a) Time distribution *t* of the magnitude *Mw* of earthquakes during the first 1000 years of one model. Both mainshocks and aftershocks are shown with black dots. Earthquakes with rupture zone extending to the surface and cutting the river, located at the middle of the fault trace, are shown with red dots. b) The cumulative (light red) and incremental (light blue) Gutenberg-Richter magnitude-frequency distribution of earthquakes for one model. *N* is the number of events and *D* is the associated displacement computed using Leonard (2010) scaling law.~~

3.2 Mainshocks

Mainshocks are generated along the fault plane. The potential magnitude range of mainshocks is bounded by fault width, that set the maximum earthquake rupture width and by a minimum rupture width, here chosen at 500 m. Based on Leonard (2010), the modeled thrust fault allows magnitudes ranging from $Mw_{min} = 3.7$ to $Mw_{max} = 7.3$. Inside these bounds, the magnitude of each mainshock is determined by randomly sampling the Gutenberg-Richter distribution, with a b-value of 1~~.~~ (Fig. 2). The earthquake productivity of the distribution is inferred based on the arbitrarily chosen rate of mainshock $R = 0.1$ day^{-1}, leading to $a = \log_{10}(R\ T) + b\ Mw_{min} = 8.975$. The time occurrence of each mainshock is randomly sampled over the duration of the simulation. Each mainshock is therefore considered independent, and the only relationship between mainshocks is that their population statistically respects the Gutenberg-Richter distribution (Gutenberg and Richter, 1944).

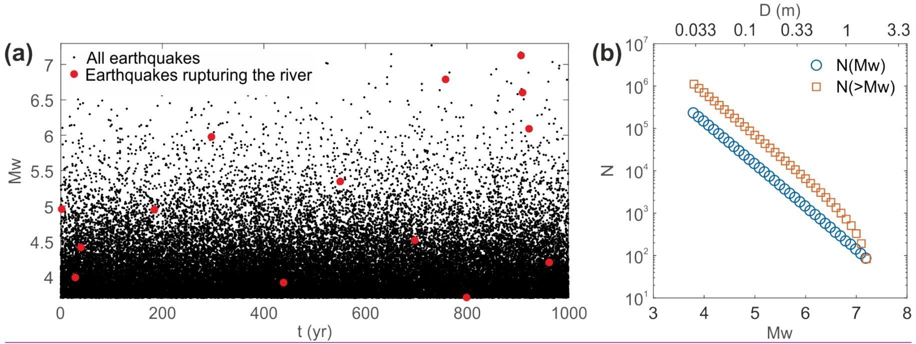

Figure 2. Modeled seismicity and its statistical characteristics. a) Time distribution *t* of the magnitude *Mw* of earthquakes during the first 1000 years of one model. Both mainshocks and aftershocks are shown with black dots. Earthquakes with rupture zone extending to the surface and cutting the river, located at the middle of the fault trace, are shown with red dots. b) The cumulative (light red squares) and incremental (light blue circles) Gutenberg-Richter magnitude-frequency distribution of earthquakes for one model. *N* is the number of events and *D* is the associated displacement computed using Leonard (2010) scaling law.

The spatial location of mainshocks inside the fault plane is sampled using a 2D distribution that correspond to a truncated normal distribution across-strike and to a uniform distribution along-strike (Fig. ~~2~~3). A normal distribution with depth roughly mimics the depth distribution of natural earthquakes in the upper crust, that ~~tend~~tends to show a maximum number of earthquakes at intermediate depth and less towards the top and the tip of the fault (e.g. Sibson, 1982; Scholz, 1998). Therefore, we set the mean of the normal distribution equal to 7.5 km of depth as the fault tip has 15 km of depth so that earthquakes are more numerous at this intermediate depth. ~~The~~ We define two end-member models, referred to as 1) the “seismic and aseismic slip” model using a variance ~~σ~~ of the normal distribution ~~is varied for the 4 considered models between~~ $\sigma = W/10$, corresponding to a narrow depth~~-~~distribution, and 2) the “only seismic slip” model with $\sigma = 3.3W$, corresponding to an almost uniform depth-distribution. ~~This latter is hereinafter referred to as the reference model.~~ We impose that the maximum earthquake frequency, at depth 7.5 km, ~~to be~~is equal in-between all the models.

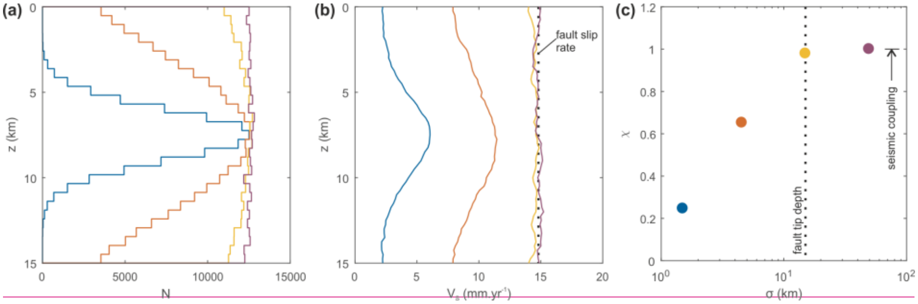

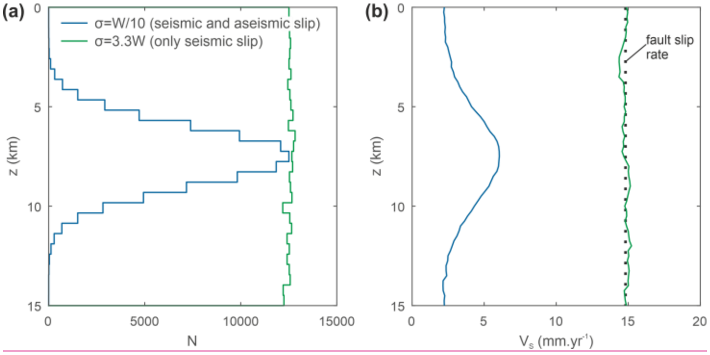

Figure ~~2~~3. Depth distribution of earthquakes, seismic and aseismic slip. a) Depth-distribution of the number N of mainshocks for the ~~4~~2 models considered here. The depth distribution is a normal one centered at 7.5 km of depth and with a variance σ equals to $W/10$ (~~light~~ blue~~), $W/3.3$ (orange), W (yellow) and~~) or $3.3W$ (~~purple~~green). b) Depth-distribution of seismic V_S slip. The vertical black line indicates the averaged fault slip rate of ~15 mm.yr^{-1}, summing seismic and aseismic slip. Aseismic slip rate is simply the difference between the average fault slip rate and seismic slip rate, so that all models share the same total slip rate. ~~c) Variation with σ of the degree of seismic coupling χ averaged along the fault. The color code, representing the different models, is the same for panels a, b and c.~~

3.3 Aftershocks

Each mainshock triggers a series of aftershocks that is determined based on the branching aftershock sequence (BASS) model (Turcotte et al., 2007). It represents an alternative to the more classical epidemic type aftershock sequence (ETAS) models (Ogata, 1988), with the advantage of being fully self-similar. We here only briefly describe the BASS model as more details can be found in Turcotte et al. (2007). Based on a mainshock, the BASS model produces a sequence of aftershocks which respect four statistical laws: 1) the Gutenberg-Richter frequency-magnitude distribution (Gutenberg and Richter, 1944; Fig.1); 2) a modified Båth's law (Shcherbakov and Turcotte, 2004), which controls the difference in the magnitude of a mainshock and its largest aftershock; 3) a generalized form of Omori's law describing the temporal decay of the rate of aftershocks (Shcherbakov et al., 2004); and 4) a spatial form of the Omori's law, that controls the spatial distribution of aftersocks (Helmstetter and Sornette, 2003). The BASS model relies on six parameters: the b-value that we set equal to $b = 1$, the magnitude difference $\Delta Mw = 1.25$ of Båth's law, the exponent $p = 1.25$ and offset $c = 0.1$ days of the temporal Omori's law, and the exponent $q = 1.35$ and offset $d = 4.0$ meters of the spatial Omori's law. The values of these aftershock parameters are based on Turcotte et al. (2007) and are constant for all the simulations performed in this paper. Seismicity along the fault is therefore made of mainshocks and their aftershocks. This aftershock model is also similar to the one developed by Croissant et al. (2019).

3.4 Earthquake rupture

The length L_{rup}, width W_{rup} and average co-seismic displacement D of each earthquake rupture, including mainshocks and aftershocks, are determined using scaling laws with seismic moment M_O, empirically determined from a set of intraplate dip-slip earthquakes (Leonard, 2010) following Eq. (2-4):

$$L_{rup} = \left(\frac{M_O}{\mu {C_1}^{3/2} C_2}\right)^{\frac{2}{3(1+\beta)}}, \tag{2}$$

$$W_{rup} = C_1 {L_{rup}}^{\beta}, \tag{3}$$

$$D = C_1^{\frac{1}{2}} C_2 {L_{rup}}^{\frac{1+\beta}{2}}, \tag{4}$$

where $C_1 = 17.5$, $C_2 = 3.8\ 10^{-5}$ and $\beta = 2/3$ are constants and $\mu = 30$ GPa is the shear modulus (Fig. 1). The location of the rupture patches around each earthquake are positioned randomly to prevent hypocenters being centered inside their rupture patches. The fault has some periodic boundary conditions, in the sense that if the rupture patch of an earthquake exceeds one of the fault limits, the rupture area in excess is continued on the opposite side of this limit. This choice maintains a statistically homogeneous pattern of fault slip rate on the fault plane in the case of the ~~reference~~"only seismic slip" model (which displays an almost homogeneous distribution of mainshocks on the fault plane). Another strategy, consisting in relocating each rupture in excess inside the fault limits, was dismissed ~~because~~as it was leading to gradients of fault slip rates close to ~~each ~~fault ~~limit~~tips.

3.~~4~~5 Seismic and aseismic slip

Slip along the fault plane is partitioned between seismic and aseismic slip. The average slip rate V_F of the fault over the duration of the simulation is given by $V_F = V_S + V_A$, where $V_S = \sum M_O/(\mu\, TWL)$ is the seismic slip, due to all the earthquakes rupturing the fault, and V_A is aseismic slip. The average degree of seismic coupling on the fault plane is $\chi = V_S/V_F$ (Scholz, 1998~~).~~) and represents the proportion of fault slip that occurs by earthquakes and seismic slip. We define the reference fault slip rate as equal to the seismic slip rate of the ~~reference~~“only seismic slip” model so that $V_F = V_S \simeq 15$ mm.yr^{-1}. This velocity is only given approximatively as the model developed here is stochastic and leads to intrinsic variability in the number and magnitude of earthquakes for the same parametrization. We follow the paradigm of statistically homogeneous long-term fault slip over the fault. The ~~reference~~“only seismic slip” model, with ~~$\sigma = 3.3W$ and~~ an almost uniform spatial distribution of mainshocks, is therefore in average fully coupled, with $\chi = 1$, while the “seismic and aseismic slip” model ~~with $\sigma = W/10$~~, displaying a large change with depth of the distribution of mainshocks, is dominated by aseismic slip with $\chi \simeq 0.25$~~ (Fig. 2).~~. In the modeling framework developed here, even a fully coupled fault can display significant spatial variations of fault slip rate. ~~Fault slip~~Slip rate on the fault plane of the ~~reference~~“only seismic slip” model varies between 11.4 to 18.2 mm.yr^{-1} for an average value of ~15 mm.yr^{-1}. However, theses spatial variations are randomly distributed and do not follow any specific pattern (Fig. ~~3~~4).

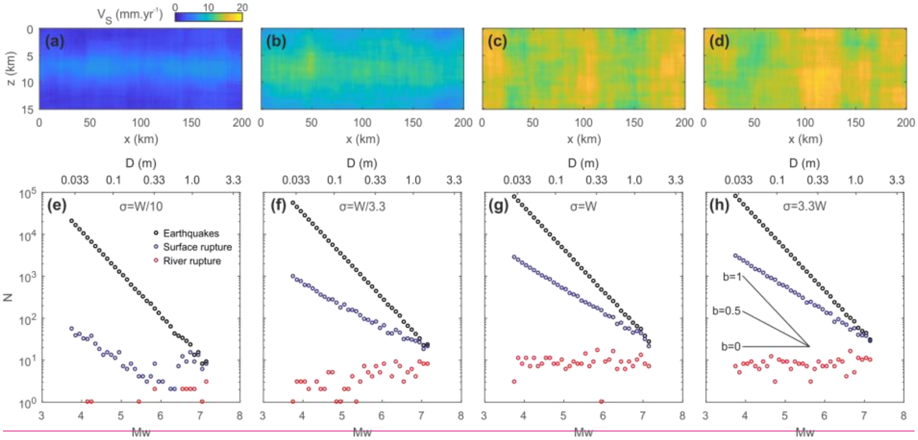

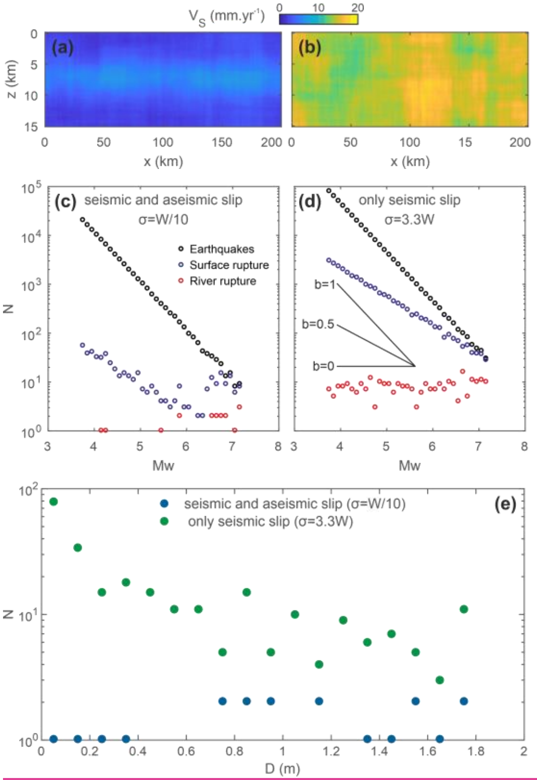

Figure ~~3~~4. Incremental distribution of earthquake magnitude and displacement in surface and at depth. ~~a-d) Map~~Maps of averaged fault seismic slip rate V_S on the fault plane for ~~models with σ equals to, from left to right, $W/10$, $W/3.3$, W and $3.3W$, corresponding to increasing degree of~~ a) the “seismic ~~coupling χ.~~and aseismic slip” and b) the “only seismic slip” models. The scale of the ~~z~~z-axis is increased compared to the ~~x~~x-axis to enhance readability. ~~e-h~~c-d) Modeled magnitude ~~or displacement~~ distributions of earthquakes on the fault (black circles), earthquakes rupturing the surface (blue circles) and of earthquakes rupturing the river (red circles) for the same ~~value of σ~~models than in panels a ~~d.~~ and b, respectively. N is here is the incremental number of earthquakes, i.e. $N(m)$. e) Distributions of displacement for earthquake rupturing the river for the considered models, with green and blue circles representing the “only seismic slip” and the “seismic and aseismic slip” models, respectively.

3.~~5~~6 River uplift

A virtual river, orientated orthogonally to the fault trace, crosses the fault trace at its center, at $x = L/2$. This river witnesses the distribution of co-seismic and aseismic displacement modifying its topography and slope. For the sake of simplicity, 1) we assume that any surface rupture generates displacement only in the vertical direction~~,~~ and 2) that co-seismic and aseismic deformation lead to a block uplift of the hanging wall, homogeneous along the river profile. These 2 assumptions clearly neglect the influence of the fault dipping angle and of the spatial distribution of uplift in surface during an earthquake, which depends mainly on earthquake magnitude, depth, geometry and on the crustal rheology. In turn, earthquakes that do not rupture the surface at the location of the river have no effect on river topography and slope in this simple model. The rate of uplift is equal to V_F at the ~~intersect~~intersection between the fault trace and the river.

3.~~6~~7 River topographic evolution

~~A classical detachment-limited approach to describe the rate of river erosion E is the stream power incision model (Howard and Kerby, 1983; Howard, 1994; Whipple and Tucker, 1999; Lague, 2014) described in Eq. (5):~~

$$\frac{dh}{dt} = V_F - E = V_F - KA^m\left(\frac{dh}{dy}\right)^n, \tag{5}$$

~~where h is the elevation of the bedrock bed of the river, t the time, y the distance along the river (i.e. across-strike the fault trace), $S = dh/dy$ the local river slope, A the upstream drainage area, K the erodibility and m and n are two exponents. Considering a linear dependency of erosion rates to slope, with $n = 1$, the stream power incision model is equivalent to a linear kinematic wave equation. Under this condition, it can be demonstrated (Rosenbloom and Anderson, 1994; Tucker and Whipple, 2002; Whittaker and Boulton, 2012; Royden and Perron, 2013) that knickpoints or slope patches along the river migrate upstream at a rate determined by Eq. (6):~~

$$V_R = \frac{dy}{dt} = KA^m. \tag{6}$$

~~Moreover, recent empirical results suggest that using $n = 1$ and $m = 0.5$ is suited to describe knickpoint migration (Lague, 2014).~~ ~~In the following, we only consider the migration of slope patches over short distances upstream, during the $T = 10\ kyr$ of the simulation.~~ ~~If the total migration distance is small compared to the entire river length, from its source to the modeled frontal thrust fault, the migration velocity V_R can be approximated as a constant. This condition holds only if $KT \ll 1$, considering that river length generally scales with about the square root of drainage area (Hack, 1957).~~ To model river erosion, we consider a simple model considering that knickpoints migrate upstream at constant velocity V_R along the y-axis, that is perpendicular to the fault trace orientated along the x-axis. We show in the Appendice A that this constant migration velocity model corresponds to a prediction of the stream power law (Howard and Kerby, 1983; Howard, 1994; Whipple and Tucker, 1999; Lague, 2014) which holds if drainage area is about constant over the region of interest. Our model is therefore appropriate to model knickpoint migration in near-fault conditions and for large drainage areas. In the following, we only consider the migration of slope patches over short distances upstream, during the T=10 kyr of the simulation. We set the horizontal retreat rate to $V_R = 0.1$ m.yr^{-1}, which corresponds to a high rate of knickpoint retreat over geological time-scales (>10^3 yr) but a moderate one over shorter time-scales (e.g. Van Heijst and Postma, 2001).~~We hereinafter consider that V_R is a constant. Assuming a steady state river profile over the length of the simulation, so that $E = V_E$, the average river slope φ just upstream the fault trace is $\varphi = (V_E/V_R)^{1/n}$.~~

Formatted: English (United Kingdom)

3.~~7~~8 Numerical implementation

Numerically, we solve in 2D the evolution of a river profile crossing a fault, subjected to slip during earthquakes and to aseismic slip. After having set the parameters, the model 1) generates mainshocks and aftershocks, including their magnitude, location and timing, and 2) computes the time evolution of the river profile subjected to uplift and erosion. Time stepping combines a regular time step, to account for uplift by aseismic slip, with the time of occurrence of each earthquake rupturing the surface at the location of the river, to account for co-seismic slip. During each aseismic time step, one node of coordinates $(h = 0, y = 0)$ is added to the river profile at the downstream end of the river (i.e. the location of the fault trace). During each co-seismic time step, two nodes of coordinates $(h = 0, y = 0)$ and $(h = D, y = 0)$ are added to the river at the downstream end of the river, to represent the vertical step associated to the co-seismic knickpoint. The remaining nodes, located upstream, are uplifted following the aseismic uplift rate V_A and potential co-seismic displacement. River erosion is accounted for by horizontal advection of river nodes following a constant velocity V_R along the y-axis. As we neglect the contribution of horizontal displacement due to fault slip, we do not consider any horizontal advection induced by tectonics, contrary to some previous studies (Miller et al., 2007; Castelltort et al., 2012; Thieulot et al., 2014; Goren et al., 2015).

4 ~~Results~~

~~4.1 Distribution~~Magnitude, displacement and temporal distributions of earthquakes~~, surface ruptures~~ and co-seismic knickpoints

Formatted: Heading 1

Formatted: English (United States)

Formatted: English (United States)

4.1 Magnitude distributions

We first use this model to investigate the distribution of ~~earthquakes, and their associated co-seismic displacement,~~earthquake magnitudes that rupture 1) the fault, 2) the surface and 3) the surface at the location of the river (Fig. ~~3~~4). For clarity, the frequency-magnitude distributions are shown as incremental distributions $N(m)$ and not as cumulative distributions $N(\geq m)$. Unsurprisingly, the frequency-magnitude distribution of earthquakes on the fault follow a negative power-law distribution with an exponent $b = 1$, ~~characteristic of~~following the imposed Gutenberg-Richter distribution~~ for the mainshocks and aftershocks.~~. Increasing the ~~variance σ of the spatial distribution of mainshocks, and in turn the~~ degree of seismic coupling χ~~,~~ only ~~shift~~shifts the distribution vertically by increasing the total number of earthquakes.

The distribution of earthquakes rupturing the surface follows a negative power law with an exponent -0.5 ~~in~~for the ~~case of the reference~~“only seismic slip” model ~~and for models~~ with a high degree of seismic coupling. In the case of the “seismic and aseismic slip” model~~ with the~~, characterized by a lower degree of seismic coupling, the distribution follows a more complex pattern. ~~For earthquakes below~~Below a threshold magnitude, here around 6, the distribution follows a negative power law with an exponent -0.5. ~~For earthquakes above~~Above this threshold magnitude, the distribution rises to reach the Gutenberg-Richter distribution and then decreases following the trend of the Gutenberg-Richter distribution. This results from the non-uniformity of the distribution of earthquakes with depth~~ for the model with a small value of σ and χ.~~. In this model, large magnitude earthquakes can rupture the surface, without requiring their hypocenters to be at shallow depth. Whereas, small magnitude earthquakes can only rupture the surface if their hypocenters are located close to the surface, which is unlikely due to the shape of the depth-distribution of mainshocks (Fig. ~~2~~3). The threshold magnitude depends on the depth-distribution of mainshocks, and particularly on its upper limit, but also on the aftershock depth-distribution that extends the range of possible depths due to Omori’s law in space.

The distribution of ~~earthquakes~~earthquake magnitude rupturing the river follows a uniform distribution for ~~models dominated by~~the “only seismic slip~~ and a homogeneous distribution of mainshocks in space~~” model. This novel result has potentially large implications as it means that a river has an equal probability of being ruptured by large or small earthquakes. This homogeneous distribution results from considering earthquake ruptures at one location and is yet consistent with a Gutenberg-Richter distribution of magnitudes along the modelled 2D fault plane. However, for ~~models with a low degree of~~ the “seismic ~~coupling~~and aseismic slip” model, mostly large-magnitude earthquakes manage to have ruptures cutting the river profile. Low-magnitude earthquakes, except for a few events, do not rupture the river. The magnitude threshold for river rupture is close to 6, similar to the one observed for surface ruptures. ~~Following Leonard (2010), a Mw 6 earthquake is characterized by a rupture length $L \simeq 12$ km, width $W \simeq 9$ and displacement $D \simeq 0.4$ m. Above a depth of 3 km, earthquakes with magnitude greater than 6 tend to become unlikely in the most aseismic model, with $\sigma = W/10$. This depth as well as the magnitude threshold decrease when increasing σ.~~ To date, there is no universal model of the depth-distribution of earthquakes and of the partitioning between aseismic and seismic slip at shallow depth for intra- or inter-plate faults (e.g. Marone and Scholz, 1988; Scholz, 1998, Schmittbuhl et al., 2015; Jolivet et al., 2015). Yet, our results, i.e. a uniform distribution of earthquake magnitude cutting the river in the fully seismic case or only large magnitude earthquakes rupturing the river for the model dominated by aseismic slip at shallow depth, clearly offer a guide to analyze river profiles in terms of fault properties.

4.2 Displacement distributions

Fault displacement D during an earthquake scales linearly with seismic moment M_O (Wells and Coppersmith, 1994; Leonard, 2010), that is related to magnitude by a logarithmic function, $Mw = 2/3\log_{10}(M_O) - 6.07$ (Kanamori, 1977). It results that a uniform distribution of earthquake magnitude, that is observed for earthquakes cutting the river in the case of the “only seismic slip” model, should lead to a negative exponential distribution of earthquake displacements. The same finding with the numerical model (Fig. 4e). In the case of the “seismic and aseismic slip” model, it is more difficult to quantitatively characterize the resulting distributions due to the lack of events, but we observe a relatively uniform distribution of surface displacements.

4.3 Temporal distributions

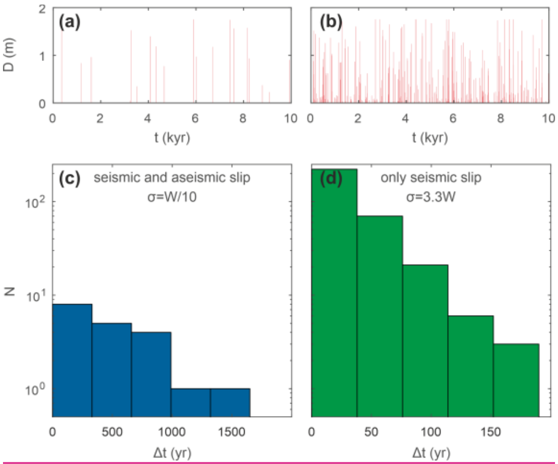

Figure 5. Time~~-~~ distribution of earthquakes rupturing the river. a-b) Co-seismic displacements D at the location of the river as a function of time t for each model. c-d) Distribution of inter-event time Δt of earthquakes rupturing the surface at the location of the river.

We now investigate the time distribution of earthquakes rupturing the surface at the location of the river and their associated displacement. The "seismic and aseismic slip" and the "only seismic slip" models ~~with $\sigma = W/10, W/3.3, W, 3.3W$~~ have 20~~, 148, 323~~ and 299 earthquakes cutting the river, respectively. Their average co-seismic displacement is 1 ~~m, 0.6 m, 0.45 m~~ and 0.5 m, respectively. This illustrates that models ~~nd~~ dominated by aseismic slip have less frequent earthquakes cutting the river, but that their average displacement is greater, due to the censoring of surface ruptures associated to low-magnitude earthquakes (Fig. 4).

Consistent with this last result, the inter-event time Δt in-between successive earthquakes cutting the river increases significantly from the ~~reference~~"only seismic slip" model ~~($\sigma = 3.3W$)~~ to the most "seismic and aseismic slip" model ~~($\sigma = W/10$).~~. In other words, the frequency of surface rupture is higher in the most seismic models and decrease with aseismic slip. This inter-event time ~~(or spacing)~~ distribution follows for each model an exponential decay (Fig. ~~4~~5), which is consistent with a Poisson process. For the "seismic and aseismic slip" model, the low number of events, 20 earthquakes, precludes characterizing a negative exponential distribution. This exponential decay implies that fault properties have no major effect on the temporal structure of earthquakes cutting a river, only on their frequency.

Formatted: Font: 9 pt, English (United States)

Formatted: Font: 9 pt, English (United States)

Formatted: English (United States)

Formatted: Normal

5 Knickpoints along single river profiles

5.1 Constant knickpoint velocity

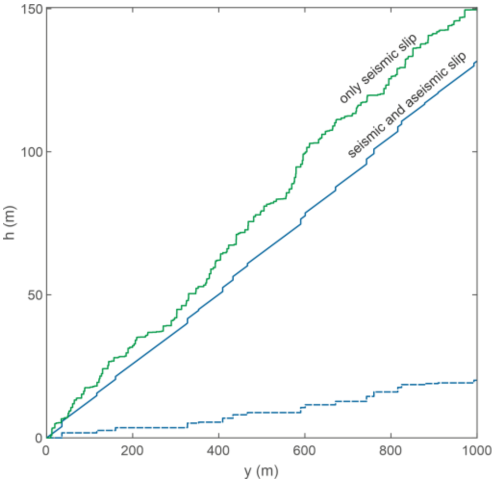

Figure 6.

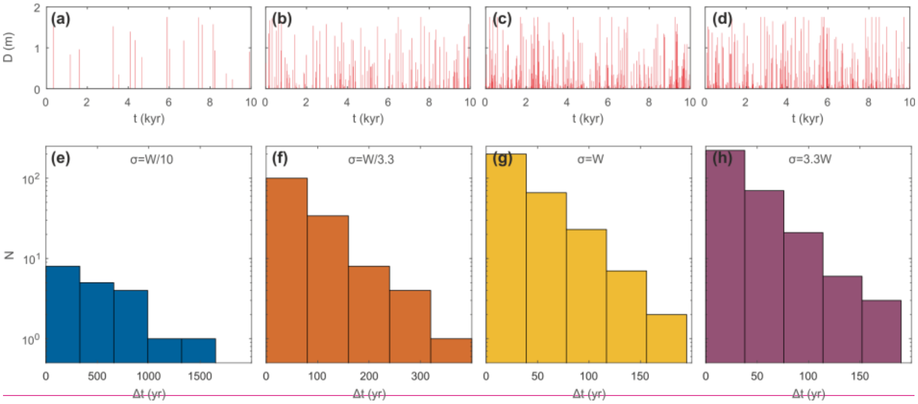

~~**Figure 4.** Time distribution of earthquakes rupturing the river. a-d) Co-seismic displacements D at the location of the river as a function of time t for each model. e-h) Distribution of inter-event time Δt of earthquakes rupturing the surface at the location of the river. Models represented have a variance σ equals to $W/10$ (light blue), $W/3.3$ (orange), W (yellow) and $3.3W$ (purple).~~

~~4.3 River profiles in near-fault conditions~~Modeled river profiles considering the “only seismic slip” (green line) and the “seismic and aseismic slip” (blue line) models. For this latter, the contribution of seismic slip is showed (dashed blue line).

If the slope patches generated by differential motion across the fault do not migrate horizontally, due for instance to a lack of erosion, the succession of earthquakes would progressively build a vertical fault scarp in this model. Here, we rather consider the case of a migrating topography due to river backward erosion following a ~~linear stream power incision~~kinematic model~~. We set the horizontal retreat rate to~~ with $V_R = 0.1$ m.yr^{-1}~~, which corresponds to a high rates of knickpoint retreat over geological time-scales (>10^3 yr) but a moderate one over shorter time-scales (e.g.~~ . It~~Van Heijst and Postma, 2001). In the model, setting $V_R = 0.1$ m.yr^{-1}~~ results in an averaged river slope just upstream the fault trace of $\varphi =$ ~~$(V_F/V_R)^{1/n} =$~~ $V_F/V_R = 0.15$ or 8.5°, with $V_F = 15$ mm.yr^{-1}~~. This horizontal retreat rate V_R can~~ (see Appendix A and ~~be obtained for an infinity of couples of the A and K parameters, following the relationship $V_R = KA^m$, that yet must at least satisfy the condition $KT \ll 1$ (~~Fig. ~~5~~A1). River~~). Other conditions exist, including the domain of validity in the A space of the stream power incision model or that the slope generated for a given value of A makes sense in terms of river steepness. However, they are not further considered as the scope of this paper is to develop a general quantitative framework to investigate slope and topographic building by a fault.~~

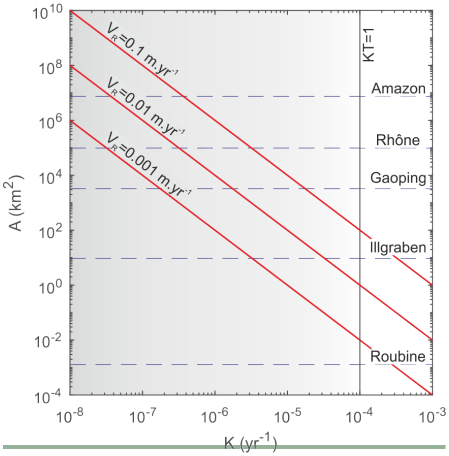

~~**Figure** 5. Range of possible couples of parameters of river drainage area A and erodability K for different values of retreat rate V_R (red lines). The vertical black line indicates the uppermost value of K, as $KT \ll 1$. The range of acceptable values of K is indicated by a gradient from white (non-acceptable) to grey (acceptable). The drainage area A of some iconic catchments are indicated with dashed blue lines and include the Amazon (south America), Rhône (Europe), Gaoping (Taiwan), Illgraben (Switzerland) and Roubine (France) rivers.~~

Formatted: Normal

Formatted: English (United Kingdom)

~~Considering these parameters, river~~ profiles are obtained for the two different models ~~with different values of σ.~~(Fig. 6). We first only consider seismic slip, so that only earthquakes rupturing the river contribute to topographic building ~~(Fig. 6a).~~. After $T = 10$ kyr of model duration, the models have resulted in about 20~~, 89, 146 and~~ to 150 m of topographic building for ~~$\sigma = W/10, W/3.3, W, 3.3W$~~the "seismic and aseismic slip" and "only seismic slip" models, respectively. The local ratio between V_S and V_F can depart from their fault-averaged values χ, due 1) to the non-homogeneous distribution of co-seismic slip on the fault for models with ~~low value σ~~significant aseismic slip and 2) to the stochasticity of each model. For instance, the "seismic and aseismic slip" model ~~with $\sigma = W/10$~~ shows an apparent ratio of $20/150 \simeq 0.13$ compared to its average value $\chi = 0.25$. Each successive co-seismic knickpoint is separated by a flat river section, due to the absence of slope building by aseismic slip. As expected, the "only seismic ~~models, with high values of σ, display~~model" displays a larger number of co-seismic knickpoint than the aseismic model. Adding aseismic slip leads to sloped reaches between each knickpoint, (Fig. ~~models, with low values of σ~~6) with slopes equal to V_A/V_F. There is obviously a larger slope variability in the models dominated by seismic slip due to a larger number of knickpoints.

5.2~~Adding aseismic slip leads to sloped reaches between each knickpoint, (Fig. 6b) with slopes equal to V_A/V_F, which decreases with σ and becomes nil for the model with no aseismic slip, i.e. for $\sigma = 3.3W$. There is obviously a larger slope variability in the models dominated by seismic slip, with high value of σ, due to a larger number of knickpoints.~~

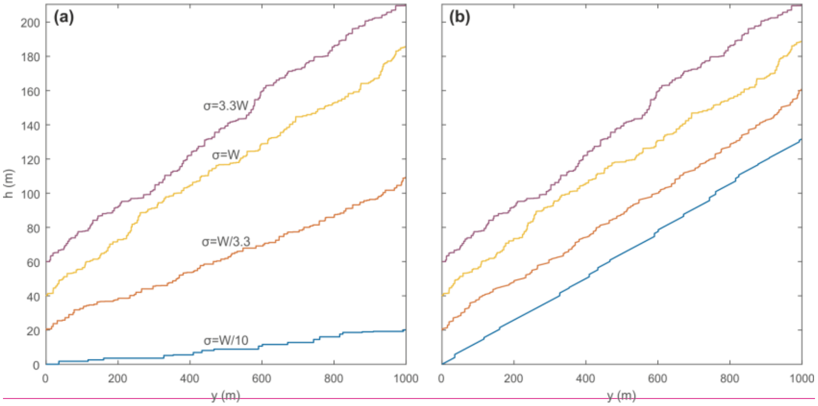

~~**Figure 6.** Modeled river profiles considering a) only seismic slip or b) both seismic and aseismic slip. Models represented have a variance σ equals to W/10 (light blue), W/3.3 (orange), W (yellow) and 3.3W (purple). River profiles are shifted vertically by an offset of 20 m to prevent potential overlap.~~

~~4.4~~ Knickpoint ~~detectability~~

~~**River profiles are used in many studies to extract co-seismic knickpoints and to assess fault activity and local to regional seismic hazard (e.g. Ewiak et al., 2015; Wei et al., 2015; Sun et al., 2016). It is therefore required to investigate whether**~~

Formatted: Heading 2

~~modeled knickpoints are statistically detectable. Knickpoint detection often relies on the use of digital elevation models and topographic data (e.g. Neely et al., 2017; Gailleton et al., 2018), which are obtained at a certain scale or resolution. The degree of detectability of each individual knickpoints~~velocity that depends ~~not only on its distance to its adjacent knickpoints, but also on the resolution, precision of the topographic data and on the roughness of the river bed.~~ on knickpoint height

Formatted: English (United Kingdom)

Formatted: English (United Kingdom)

~~Classical resolution for topographic data available at the global scale (e.g. SRTM or ASTER) are between 10 and 100 m, with precision not better than a few meters and potentially worse in narrow bedrock gorges. Local to regional topographic datasets obtained from current airborne Lidar or photogrammetric data, or derived from aerial or satellite imagery (e.g. Pléiades), display a resolution between 0.5 to about 1-5 m and a typical vertical precision of 10 cm above water. Moreover, in the vertical direction, knickpoint detectability depends also on the inherent bed roughness, mean alluvial deposit thickness and to the local distribution of sediment grain size. Sediment grains of dimension greater than 0.1 m are commonly found in rivers located in mountain ranges (e.g. Attal and Lavé, 2006), especially at low drainage areas, and there is often a thin layer of sediment covering the channel bed at low-flow potentially hiding features. If we fully acknowledge the role of river roughness, we here focus on the issue of detectability relative to topographic resolution and precision, for the sake of simplicity.~~

~~In terms of vertical precision, a precision of 0.1 m (e.g. Lidar) enables to detect knickpoints produced by an earthquake down to magnitude 4.8 (Fig. 3). For rivers permanently under water, traditional airborne Lidar using near infrared laser or photogrammetric data cannot measure river bathymetry imposing a detectability level and an uncertainty of knickpoint height of the order of the water depth. Topographic data with a precision of about 1 m would only enable to detect knickpoints for earthquakes of magnitude above 6.8. SRTM or ASTER data have precisions of a few meters, at best, that would only enable the potential detection of earthquakes of magnitude ~8 or more.~~

~~In terms of resolution, for low values of σ, each co-seismic knickpoint is generally detectable, due to the large spacing between successive knickpoints. However, for high-values of σ, some knickzones are likely made of series of knickpoints. The distribution of horizontal distance between successive knickpoints (that scales with the distribution of inter-event times), for the reference model with $\sigma = 3.3W$, shows that knickpoint inter-distance ranges between few centimeters to up to few tens of meters (Fig. 7). Using a resolution of 10 or 100 m leads to pixels including up to 22 or 70 co-seismic knickpoints, with mean values of 6 or 60 knickpoints, respectively (Fig. 7). At 1 m of resolution, the mean number of knickpoints per pixel is 0.6 (as several pixels include no knickpoints) and 23% of the pixels include more than one knickpoints. At 0.1 m of resolution, detectability becomes good and only a negligible proportion of pixels include more than one knickpoint. Increasing knickpoint retreat rate V_R by a factor 10 would favor detectability at a resolution increased by the same factor, and 1 m would become a suitable resolution instead of 0.1 m. Decreasing V_R by a factor 10 would in turn require to use a resolution of 1 cm, that is currently only reached by terrestrial Lidar data or close-range photogrammetric data. Anyhow, at such resolution, river bed roughness would probably be the limiting factor.~~

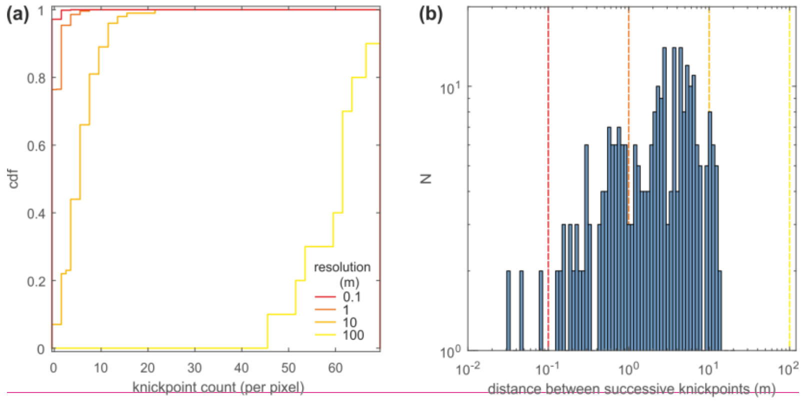

~~**Figure 7.** Spatial detectability of individual knickpoints for the reference model with $\sigma = 3.3W$. a) Cumulated distribution function (cdf) of the number of knickpoints per pixel using a resolution of 0.1 (red), 1 (dark orange), 10 (light orange) and 100 m. b) Distribution of distance between successive knickpoints using logarithmic binning. The resolutions used in panel (a) are indicated using vertical dashed lines of the same color than in a.~~

~~4.5 Knickpoint correlation in-between several parallel rivers crossing the fault~~

~~We now explore the degree of spatial correlation in between the topographic profiles of several parallel rivers flowing across-strike the fault trace. Paleo-seismological studies using knickpoints to infer fault activity generally consider the distributions of knickpoints along several sub-parallel rivers to lead to statistically robust analyses and to assess the spatial extent of each past-earthquake (e.g. Ewiak et al., 2015; Wei et al., 2015; Sun et al., 2016). Correlating topography and knickpoints along the strike of a fault, using parallel rivers, also offers an independent mean to assess the rupture length and the magnitude of a past-earthquake. Using multiple rivers is also less likely to be biased through the artificial merging of several co-seismic displacement into one detectable knickpoint in a single river (Fig. 7).~~

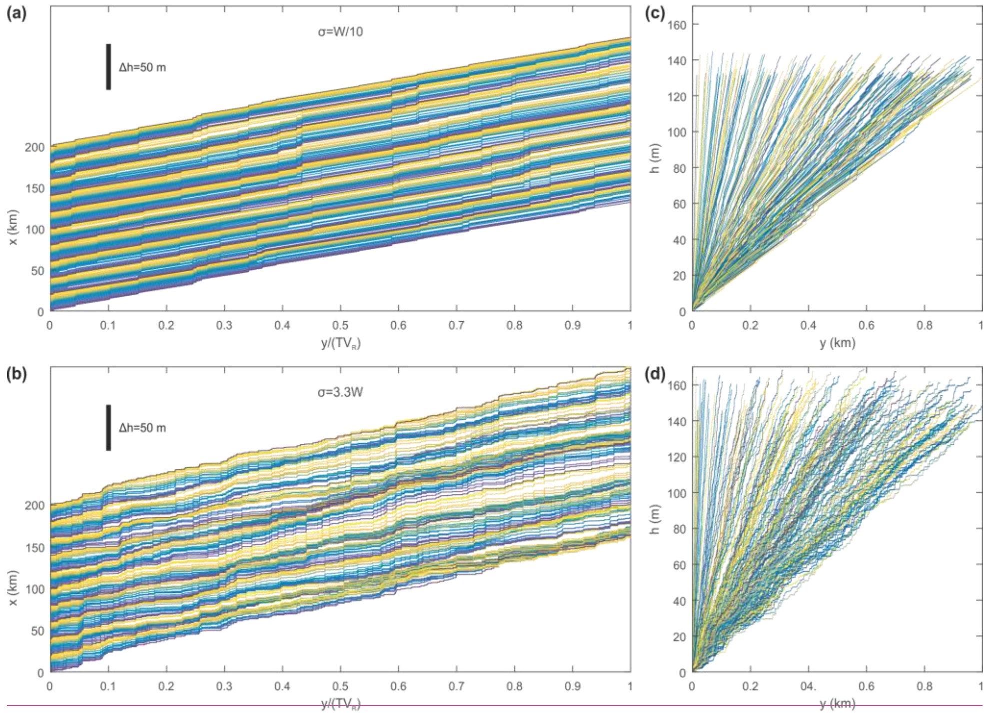

~~**Figure 8.** Topography of a set of parallel rivers flowing across-strike the fault. a-b) River profiles of 200 rivers separated by 1 km along the strike of the fault, i.e. the x-direction. River elevation h is given along the same axis, with a scaling factor of 1000. River length y across the strike of fault is normalized by knickpoint migration rate V_R times the duration of the simulation T. Non-normalized river profiles are shown on panels c and d. The colorscale is only present to help figure readability.~~

Formatted: Font: +Body (Times New Roman)

~~We therefore consider a set of rivers separated by $\Delta x = 1$ km along the strike of the fault, i.e. the x-direction. Because 1) the drainage area of each of these rivers can vary by orders of magnitude and 2) because knickpoint retreat rates show a high variability, their knickpoint migration rate V_R is randomly sampled between the range 0.001 to 0.1 m.yr^{-1}. For simplicity, we only consider the reference model, with $\sigma = 3.3W$, and the model with $\sigma = W/10$, that represent two end-members models (Fig. 8). Each profile of the 200 rivers share some common topographic characteristic, including their average number of knickpoints and total elevation. However, their average slopes and the horizontal position y of the knickpoints largely differ due to the large range of considered knickpoint retreat rate V_R. Knowing *a priori* V_R and the duration T of the simulation (i.e. or the age of the knickpoints) makes it possible to define a normalized horizontal position relative to the fault, $y/(TV_R)$.~~

~~Practically, several studies normalized by the square root of drainage area, as drainage area is generally used as a proxy for retreat rate (e.g. Crosby & Whipple, 2006). Knickpoints generated at the same time, along different rivers with different retreat rate, share the same normalized distance relative to the fault (Fig. 8a,b). This representation is convenient to assess the spatial extent of an earthquake rupturing several rivers along-strike. Non-normalized river profiles are shown on Figure 8 c and d. This representation also allows the assessment of the degree of correlation of the river profiles. Obviously, there is no significant topographic correlation when considering rivers with such a high variability in retreat rates, e.g. 0.001 to 0.1 m.yr^{-1}. We therefore compute the matrix of correlation between each river elevation profile using the river normalized horizontal distance (Fig. A1). River elevation is corrected or "detrended" from its average slope to remove an obvious source of topographic correlation. We then compute the average coefficient of correlation for a given river inter-distance Δx ranging from 0 to 100 km (Fig. 9). The two models, with $\sigma = W/10$ or $3.3W$ show a similar pattern, with a significant positive correlation (>0.5) for rivers separated by less than 14 to 23 km (10 to 45 km if accounting for the standard deviation). The maximum distance over which a correlation is expected corresponds to about 35 km, half the maximum co-seismic rupture length of ~70 km along the considered fault. This illustrates that knickpoints should not be correlated for rivers separated by more than this distance, considering the tectonic setting of this model, and fault dimensions. Detrended river profiles becomes uncorrelated or even anti-correlated starting for an inter-distance greater than about 40 km, which is slightly greater than half the maximal rupture length on the fault generated by an earthquake of magnitude 7.3. This correlation distance could increase using a wider fault generating larger magnitude earthquake with longer surface rupture. We also find that the correlation is better for the model with $\sigma = W/10$, dominated by aseismic slip and showing less knickpoints, than the reference model, with $\sigma = 3.3W$ and only seismic slip (Fig. A1). Positive correlations were obtained using horizontal distance normalized by retreat rate. However, using only catchments with similar retreat rates would also lead to positive and significant correlation even when using non-normalized distance.~~

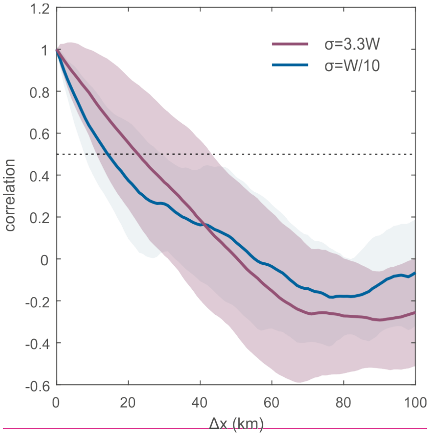

~~**Figure 9.** Similarity of river profiles along the strike of the fault. Change of the average coefficient of correlation in-between rivers located along the strike of the fault, with river inter-distance Δx. The double standard deviation is shown by the extent of the shaded area. In blue, the reference model with $\sigma = 3.3W$, and in purprle the model with $\sigma = W/10$. The average coefficient of correlation and its standard deviation are measured along the diagonals of the correlation matrix (Fig. 8). The matrices of correlation between each river profile using normalized distances are shown on Figure A1.~~

~~5 Discussion~~

~~5.1 Model limitations~~

~~To approach the problem of co-seismic knickpoint formation and their impact of river profile, we have made several simplifying assumptions. The spatial and temporal distribution of earthquakes, including mainshocks and aftershocks, only follow classical statistical and scaling laws. Fault stress state or friction properties, which are first order controlling factors of earthquake triggering (e.g. Scholz, 1998), are not explicitly accounted for. Earthquake ruptures are assumed to be rectangular, to have dimensions scaling with seismic moment and to display a homogeneous displacement (Leonard, 2010), while natural ruptures display more variable behaviors. For instance, the height of co-seismic knickpoints formed during the 1999 Mw 7.6 Chi-Chi earthquake in central Taiwan ranged from 1 to 18 m (Yanites et al., 2010). The relative contributions of seismic and aseismic processes to fault slip, and their spatial distributions, are defined in a relatively ad hoc manner, i.e. by the means of a normal distribution with depth. More specifically, fault periodic boundary conditions for earthquake ruptures are defined to enforce that a uniform distribution of earthquakes lead to a statistically uniform distribution of seismic fault slip. In addition, co-seismic displacement follows a block uplift mechanism, which contradicts observations and neglects the elasticity of the lithosphere. Yet, it is to be emphasized that block uplift in near fault conditions for large-magnitude earthquakes corresponds to an asymptotic behavior. A more realistic approach is to compute the surface displacement induced by each earthquake using for instance dislocations embedded into an elastic half-space (e.g. Okada, 1985). This alternative approach would also have the benefit of accounting for the surface displacement of earthquakes that do not rupture the surface. Moreover, surface rupture only occurs along a single fault and does not account for off-fault damage (e.g. Zinke et al., 2014), that could also generate knickpoints, or for more complex rupture geometry (e.g. Romanet et al., 2018). Surface rupture and displacement were only considered in the vertical direction, clearly simplifying the variability in the orientation of natural surface ruptures. If this paper is focused on the vertical expression of fault along river profiles, future work should account for the influence of horizontal tectonic displacement on river profile (e.g. Miller et al., 2007). Knickpoint lateral propagation along the river profile was modeled using a constant velocity, which corresponds to an asymptotic behavior of the stream power incision model for small migration distance respective to the square root of river drainage area. If the migration of knickpoints or slope patches are classically modeled using the stream power incision model (Rosenbloom and Anderson, 1994; Whittaker and Boulton, 2012; Royden and Perron, 2013), this approach was recently questioned by experimental results suggesting no obvious dependency~~

~~of the migration rate to river discharge (Baynes et al, 2018). Mechanistic models of waterfall erosion and retreat offer another more accurate but more complex approach (Scheingross and Lamb, 2017).~~

~~5.2 Model and results applicability to normal and strike-slip faults~~

~~The developed model, that was applied in this study to a continental thrust fault, can also be directly applied to a normal fault. Indeed, the adopted scaling relationships between earthquake rupture dimensions or displacements and seismic moment (Leonard, 2010) apply to dip-slip intraplate earthquakes and therefore to both normal and thrust faults. The main differences are the polarity of motion between hanging and foot wall, and the dipping angle of the fault. This latter difference vanishes in the developed approach as we assume that rupture displacement occurs only in the vertical direction. Under these limitations and simplifications, all the obtained results in this paper can be therefore directly transcribed to normal faults. Because normal faults tend to have a larger dipping angle, close to 60° in average, than thrust faults, the approximation of purely vertical co-seismic displacement is less incorrect for normal faults. Moreover, strike-slip faults or dip-slip interplate faults can also be accounted for by this model, by simply tuning the parameters of the rupture scaling laws, i.e. $\boldsymbol{C_1}$, $\boldsymbol{C_2}$, and $\boldsymbol{\beta}$. Assuming the depth-distribution of seismicity along different types of faults is identical (a likely incorrect hypothesis), changing the type of fault would not have a major impact on the results presented in this paper.~~

~~5.3 Knickpoint height distribution as a paleoseismiological tool?~~

~~Co-seismic knickpoints are common geomorphological markers found in seismic areas (Boulton and Whittaker, 2009; Yanites et al., 2010; Cook et al., 2013). Several studies have offered constraints on fault seismogenic activity from the study of river profile and knickpoint height (Boulton and Whittaker, 2009; Ewiak et al., 2015; Wei et al., 2015; He and Ma, 2015; Sun et al., 2016). Natural distributions of knickpoint height are systematically dominated by large heights, corresponding to earthquake magnitudes greater than 5. For instance, the magnitude of earthquakes deduced from knickpoints extracted along rivers crossing the Atacama Fault System, follows a bell shape distribution favoring large magnitude 5.8-6.9 earthquakes (Ewiak et al., 2015). Because the distributions of knickpoints was found to share similarities with the distribution of ruptures directly along the fault scarp, this rules out the hypothesis of fully eroded co-seismic knickpoints generated by small magnitude earthquakes (Ewiak et al., 2015). This observation, of knickpoints dominated by large earthquakes and the censoring of small magnitude earthquakes, is similar to the results obtained in this paper with the model dominated by aseismic slip at shallow depth (Fig. 3e). Alternative explanations for the apparent lack of small knickpoints or scarp ruptures in most natural datasets (Ewiak et al., 2015; Wei et al., 2015; He and Ma, 2015; Sun et al., 2016) include 1) the difficulty to detect the limited displacement induced by earthquakes of magnitude 5 or less, relatively to river bed rugosity, and 2) the fault burial mechanism (Finnegan and Balco, 2013; Malatesta and Lamb, 2018) that filters out small co-seismic surface ruptures. In any case, the depth-distribution of earthquakes and of their rupture extent exert fundament control on the resulting height distribution of co-seismic knickpoint.~~

~~In turn, our results suggest that knickpoint datasets, that will become more and more accessible thanks to high-resolution topographic data, can be used to assess fault activity. Obviously, the height of knickpoints provide some form of evidence for the earthquakes that have generated them. Moreover, a uniform distribution of knickpoint height points toward a purely seismic fault, while a bell-shaped distribution suggests aseismic slip or even a slip deficit at shallow depths. The main limitation is yet the poorly known impact of geomorphological processes on evolution of the shape of knickpoints. Some knickpoints along the Atacama Fault System have a reduced height compare to their initial rupture (Ewiak et al., 2015), while some knickpoints produced during Chi-Chi earthquake in 1999 were higher 10 years later (Yanites et al., 2010). These contrasting cases illustrate some potential, and poorly understood, pitfalls in using knickpoints to infer fault and seismic activity.~~

~~5.4 River dynamics: constant uplift or time-variable uplift with earthquakes?~~

~~Most numerical efforts attempting at modeling the long-term (>10-100 kyr) topographic building of mountainous or rift settings have used a constant or smoothly varying uplift rate (e.g. Braun and Willett, 2013; Thieulot et al., 2014; Campforts et al., 2017), not including the variability of uplift rate during the seismic cycle. If using a stream power incision model with a linear dependency to slope $n = 1$, this choice is acceptable as the variability of uplift rate and the associated variability of slope patches shaped throughout the seismic cycle can be averaged out. Moreover, knickpoint retreat rate is in this case independent of slope as this model corresponds to a linear kinematic wave equation, (Rosenbloom and Anderson, 1994; Tucker and Whipple, 2002; Whittaker and Boulton, 2012; Royden and Perron, 2013). However, if using a non-linear dependency of erosion rates to slope, with $n \neq 1$, and only considering a long-term averaged uplift rate, and not its variability, is an approximation that becomes more incorrect with the degree of non-linearity of the model. In other words, the erosion rate of a river profile made of co-seismic knickpoints separated by low-slope river sections built during aseismic periods (Fig. 6,8) is not equivalent to the erosion rate of a smooth river profile with the same average slope and built under a constant uplift rate. In a non-linear stream power incision model, the retreat rate is sensitive to slope at a power $n - 1$. For $n > 1$, greater slope patches will migrate quicker than lower slope patches, and vice versa for $n < 1$. While a large proportion of the literature considers the linear stream power incision model (or the unit stream power model) as the reference model, the parametrization of the stream power incision and in particular of the slope exponent n is still an open debate, as is its actual applicability to model knickpoint migration (e.g. Lague, 2014). Moreover, the physics of knickpoint or waterfall retreat likely depends on other variables such as knickpoint height (Holland and Pickup, 1976; Hayakawa and Matsukura, 2003; Haviv et al., 2010; Scheingross and Lamb, 2017), sediment supply (Jansen et al., 2011), lithological structure (Lamb and Dietrich, 2009), and lithological strength (Baynes et al., 2018). Even if this debate is clearly out of the scope of this paper, the implication of this study for the understanding of river erosion and dynamics should not be ignored. The modelling results of this study show that the frequency-displacement distribution of earthquakes rupturing a river is uniform for purely seismic faults and follows a bell shape, favoring large rupture associated to large magnitude earthquakes, for faults with significant shallow aseismic slip. This result offers a complementary - not an alternative – explanation to the fault-burial mechanism (Malatesta and Lamb, 2018) for the apparent larger proportion of high waterfalls.~~

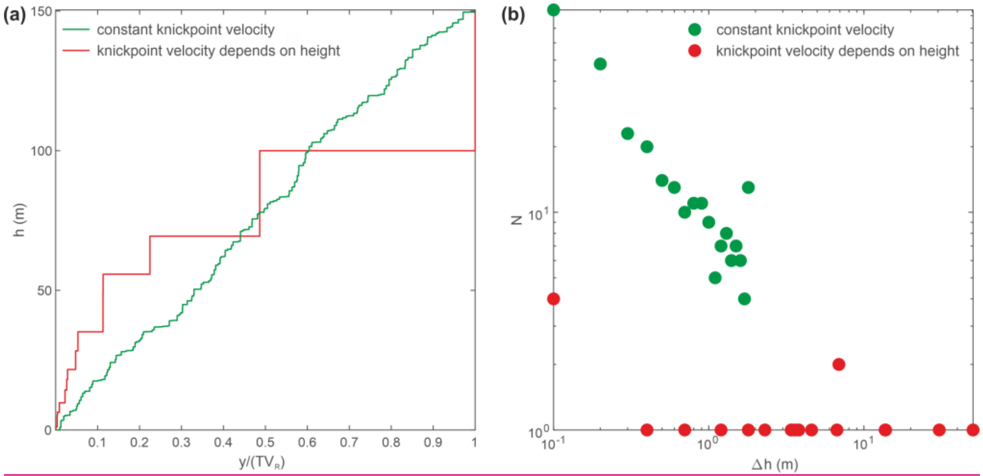

Figure 7. ~~5.5~~Modeled a) river profiles and b) knickpoint height distribution considering a constant knickpoint velocity (green line and circles) or a velocity depending on knickpoint height (red line and circles) .

Even if most simulations of this paper are done with a simple kinematic model using a constant knickpoint velocity, we now consider a model with a knickpoint velocity that depends on knickpoint height with $V_R = r(1 + \Delta h/\Delta h_0)^q$, where d is a constant, set to the previously used constant knickpoint retreat rate 0.1 m.yr^{-1}, Δh the knickpoint height, $\Delta h_0 = 1$ m a reference knickpoint height and $r = 0.1$ an exponent representing the sensitivity of knickpoint velocity to knickpoint height. This model is motivated by mechanical arguments suggesting a dependency of knickpoint velocity to their height (Scheingross and Lamb, 2017). We allow a quicker knickpoint of height Δh_i that encounters a slower knickpoints of height Δh_j to merge, forming in turn a single knickpoint of height $\Delta h_i + \Delta h_j$ and of greater speed than the former knickpoints. The resulting river profile can be compared to the one obtained with the "only seismic slip" model (Fig. 7a). The dependency of knickpoint speed to height leads to a river profile with high but seldom knickpoints. The inter-distance between successive knickpoints increases with total retreat. Small knickpoints only survive close to the fault before being "eaten" by quicker and higher knickpoints during their retreat. Only the highest knickpoints, reaching tens of meters of height, survive after a significant distance of retreat. This behavior is also evidenced when comparing the distributions of knickpoint heights for these two models (Fig. 7b). The dependency of knickpoint velocity to height leads to very few knickpoints, with however a large proportion of them having a metric or decametric scale. This highlights that even limited non-linearities in the knickpoint retreat model can lead to river profiles with significant differences.

5.3 Sediment cover, fault burial and knickpoint formation

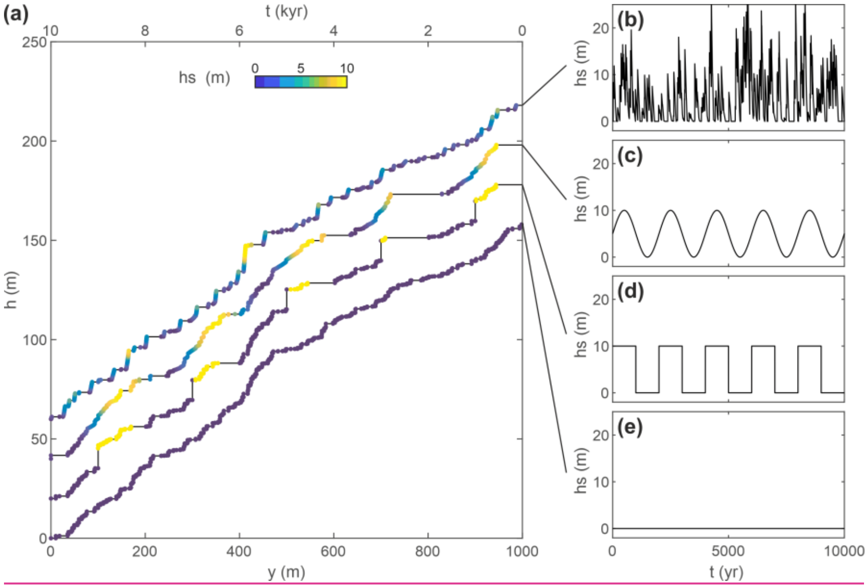

Figure 8. Impact of fault burial by sediment cover on river profile. a) River profiles are generated with no sediment cover ($hs = 0$, see panel e), with step-like temporal variations for sediment cover with a periodicity of 2 000 yr (see panel d), with sinusoidal temporal variations for sediment cover with a periodicity of 2 000 yr, mimicking climatic changes (see panel c), with a temporal variation of sediment cover induced by earthquakes (see panel b). The mean sediment cover thickness, hs, is equal to 5 m in b, c and d. River profiles are indicated with black lines and the sediment cover thickness at the time of knickpoint formation is indicated by the color of the points.~~In this paper, we~~ For readability issue, the river profiles are shifted by 20 m on panel a.

We have neglected up to now the role of sediments and their impact on knickpoint formation. More specifically, fault scarps can remain buried during the aggradation phase of an alluvial fan located immediately downstream of the fault (e.g. Carretier and Lucazeau, 2005). This mechanism is suggested to be a primary control of knickpoints and waterfalls formation by allowing the merging of several small co-seismic scarps formed during burial phases into single high-elevation waterfalls that migrate during latter incision phases (Finnegan and Balco, 2013; Malatesta and Lamb, 2018). We test this mechanism and its impact on river profiles using a simple description of fault burial by sediment cover (Fig. ~~10~~8). At each time step, the formation of a knickpoint can only occur if the fault scarp height, $h(y = 0)$, is greater than the sediment thickness of the alluvial fan, hs. In this case, the formed knickpoint height is simply $h(y = 0) - hs$.

Formatted: Font: +Body (Times New Roman)

Temporal variations of sediment thickness are prescribed using 4 scenarios: 1) no sediment cover, $hs = 0$, corresponding to the reference model (Fig. ~~10a~~8e); 2) a square wave (or step-like) function with a periodicity of 2 000 yr and a maximum amplitude of 10 m (Fig. ~~10b~~8d); 3) a sinusoidal function with a periodicity of 2 000 yr and a maximum amplitude of 10 m (Fig. ~~10c~~8c); and 4) an earthquake-driven sediment cover, where sediment increase instantaneously after each earthquake that rupture the river with an amplitude arbitrarily defined proportional to $(Mw - 5)^2$, followed by a linear decrease over 100 yr, following results by Croissant et al., 2017 (Fig. ~~10d~~8b). This last scenario mimics, in a very simplified manner, the potential transient response of an alluvial fan to the observed increase of river sediment load induced by earthquake-triggered landslides (Hovius et al., 2011; Howarth et al., 2012; Croissant et al., 2017). ~~Whereas~~Alternatively, the periodic ~~scenarios~~scenario mimics the potential response of sediment thickness to some climatic cycles. These scenarios are purely illustrative and do not aim at offering an accurate description of the impact of tectonic or climatic changes on sediment cover dynamics. For each scenario, except the one with no sediment cover, the mean sediment thickness is 5 m. For the sake of simplicity, we only consider ~~the reference model, with $\sigma = 3.3W$ and~~ “only seismic slip~~,~~” model with the same temporal sequence of earthquakes in each of the 4 scenarios. Knickpoint velocity is kept constant and equals to $V_R = 0.1$ m.yr^{-1}.

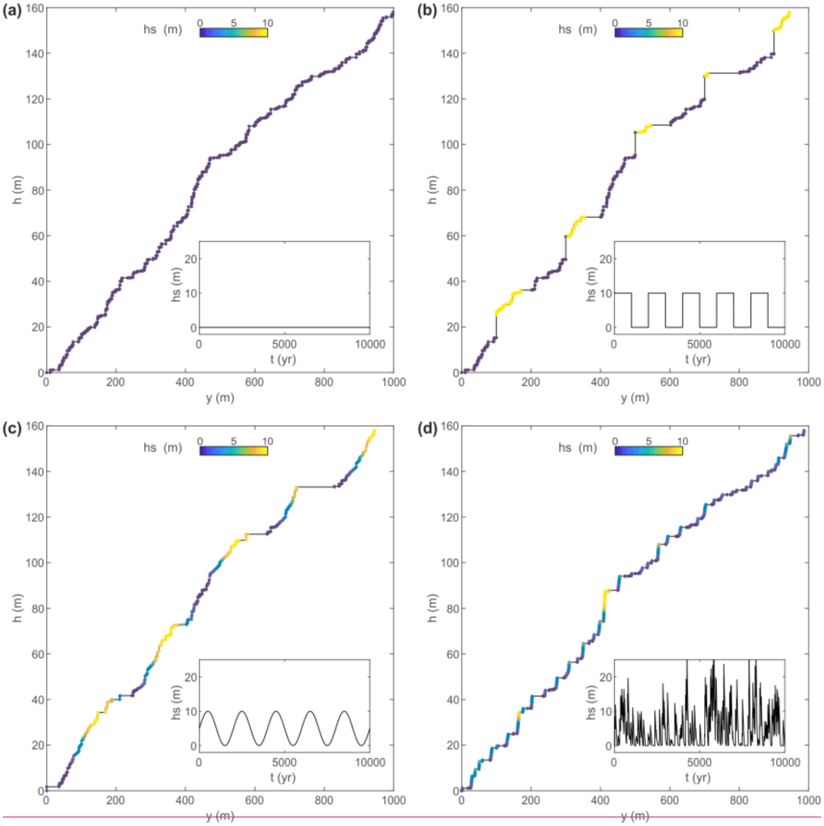

~~**Figure 10.** Impact of fault burial by sediment cover on river profile. a) River profile simulated with no sediment cover (*hs* = 0, see inset). b) River profile simulated with step-like temporal variations for sediment cover (see inset), with a periodicity of 2 000 yr. c) River profile simulated with sinusoidal temporal variations for sediment cover (see inset), mimicking climatic changes, with a periodicity of 2 000 yr. d) River profile simulated with a temporal variation of sediment cover induced by earthquakes (see inset). The mean sediment cover thickness, *hs*, is equal to 5 m in b, c and d. River profiles are indicated with black lines and the sediment cover thickness at the time of knickpoint formation is indicated by the color of the points.~~

Formatted: Font: Times New Roman

The square wave model is useful to assess the impact of ~~brutal~~abrupt changes in sediment thickness. During the phase of a high sediment cover thickness that lasts 2 000 yr, the scarp progressively builds its height until reaching 10 m during successive fault ruptures. Over this period, there is no knickpoint formation while previously formed knickpoints continue to migrate upstream, leading to elongated flat river reaches upstream of the fault. Once the scarp is re-exposed, the following earthquakes generate knickpoints (yellow dots in Fig. ~~10b~~8a), with their individual height corresponding to each associated earthquake displacement. Then, the ~~brutal~~abrupt transition from 10 m of sediment thickness to no sediment thickness suddenly exposes 10 m or more of fault scarp that forms a migrating knickpoint of elevation much higher that the largest earthquake displacement, i.e. 1.8 m. Then during the 2 000 yr that follow, with no sediment cover, each earthquake rupture generates a new knickpoint (blue dots in Fig. ~~10b~~8), as in the reference model ~~(Fig. 10a).~~ .

The sinusoidal model, mimicking climatic oscillations (Fig. ~~10c~~8c), displays a relatively similar behavior, ~~excepts~~except that it does not form 10 m high knickpoints during the phase of degradation of the sediment cover. Instead, this phase leads to the formation of "climatic knickpoints" as the rate of decrease in sediment thickness is greater than the rate of scarp building by fault slip. For the exact same reason, the phase of sediment aggradation is characterized by no knickpoint formation and by flat river reaches. Knickpoint formation and the signature of the river profile are therefore dominated by the climatic signal controlling sediment aggradation-degradation phases rather than by fault slip.

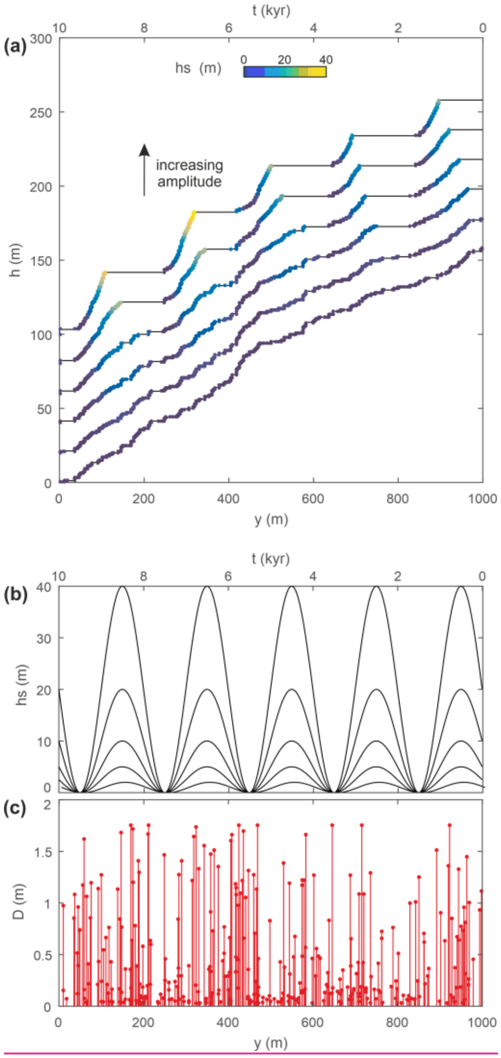

Figure 9.~~Last, the earthquake-driven sediment cover model (Fig. 10d) also leads to rate of sediment aggradation significantly higher than fault slip. As in the square-wave model, transition from no to a large sediment occurs instantaneously after each~~

~~earthquake of large magnitude. As a result, the fault becomes buried and leads to flat river reaches. Yet, because the post-seismic sediment cover degradation occurs on prescribed timescales of only 100 years, these flat river reaches are less elongated. Most knickpoints are in turn formed during phases of sediment cover degradation, that rapidly exposes fault scarp. This led to closely spaced knickpoints that formed steep knickzones. The overall river morphology differs significantly from the case with no sediment cover. The main relationship between earthquakes and knickpoints is through the co- and post-seismic sediment modulation of knickpoint formation and not through scarp building by earthquake rupture.~~

~~In these scenarios, the fault-burial mechanism by sediment cover does not necessarily lead to knickpoints with elevation greater than earthquake ruptures, except for very brutal removals of sediment cover such as in the square-wave model. Yet, in all these models, the fault-burial mechanism limits the periods of differential topography building, leading in turn to succession of steepened river reaches or knickzones, corresponding to periods of sediment removal, alternating with low slope river reaches, corresponding to periods of sediment aggradation.~~ Figure 11 ~~illustrates the role of sediment cover in modulating the surface expression of tectonics and co-seismic displacement. For the highest rates of sediment aggradation and removal, river profiles are dominated by the temporal evolution of the sediment cover and not by the activity of the fault. Whereas, for limited sediment aggradation and removal rates, the river profiles and the succession of knickpoints are dominated by the temporal occurrence of earthquakes and not by the temporal evolution of the sediment cover. These results are consistent with the ideas developed by Malatesta and Lamb (2018).~~

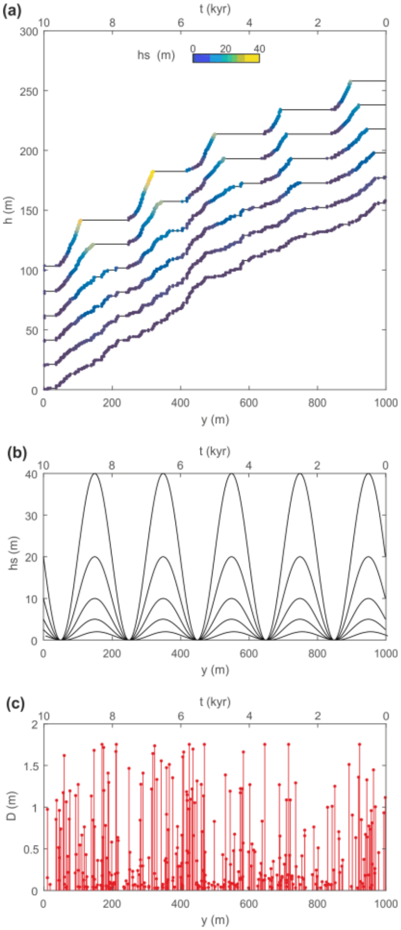

~~**Figure 11.**~~ Impact of the rate of sediment aggradation and fault burial on river profile. a) River profile simulated with sinusoidal temporal variations for sediment cover, mimicking climatic changes, with a periodicity of 2 000 yr, and an amplitude of 0, 1, 2.5, 5, 10 and 20 m. River profiles are indicated with black lines and the sediment cover thickness at the time of knickpoint formation is indicated by the color of the points. b) Time evolution of the sediment cover hs for the different simulations presented in a. c) Co-seismic displacements D at the location of the river as a function of time t for each model. For a, b and c the x-axis indicates both the distance y along the river and the corresponding time t, to relate visually fault displacement, sediment cover and river profile. Time and distance along the river are related through the knickpoint retreat rate $V_R = \frac{y}{t}$.

Formatted: Font: Bold

~~5.6~~In these scenarios, the fault-burial mechanism by sediment cover does not necessarily lead to knickpoints with elevation greater than earthquake ruptures, except for abrupt removals of sediment cover such as in the square-wave model. Yet, in all these models, the fault-burial mechanism limits the periods of differential topography building, leading in turn to succession of steepened river reaches or knickzones, corresponding to periods of sediment removal, alternating with low slope river reaches, corresponding to periods of sediment aggradation. Figure 9 illustrates the role of sediment cover in modulating the surface expression of tectonics and co-seismic displacement. For the highest rates of sediment aggradation and removal, river profiles are dominated by the temporal evolution of the sediment cover and not by the activity of the fault. Whereas, for limited sediment aggradation and removal rates, the river profiles and the succession of knickpoints are dominated by the temporal occurrence of earthquakes and not by the temporal evolution of the sediment cover. These results are consistent with the ideas developed by Malatesta and Lamb (2018).

6 Knickpoints along successive parallel rivers

6.1 From single to several parallel rivers

We now explore the degree of spatial correlation in between the topographic profiles of several parallel rivers flowing across-strike the fault trace. For the sake of simplicity we ignore the role of sediment cover on knickpoint formation and use a constant knickpoint velocity. Paleo-seismological studies using knickpoints to infer fault activity generally consider the distributions of knickpoints along several sub-parallel rivers to lead to statistically robust analyses and to assess the spatial extent of each past earthquake (e.g. Ewiak et al., 2015; Wei et al., 2015; Sun et al., 2016). Correlating topography and knickpoints along the strike of a fault, using parallel rivers, also offers independent means to assess the rupture length and the magnitude of a past earthquake. Using multiple rivers is also less likely to be biased by potential heterogeneities occurring along single rivers. We therefore consider a set of rivers separated by $\Delta x = 1$ km along the strike of the fault, i.e. the x-direction. Because 1) the drainage area of each of these rivers can vary by orders of magnitude and 2) because knickpoint retreat rates show a high variability, their knickpoint migration rate V_R is randomly sampled between the range 0.001 to 0.1 m.yr^{-1}. Each profile of the 200 rivers share some common topographic characteristic, including their average number of knickpoints and total elevation (Fig. 10). However, their average slopes and the horizontal position y of the knickpoints largely differ due to the variability of V_R. Knowing *a priori* V_R and the duration T of the simulation (i.e. the age of the knickpoints) enables to define a normalized horizontal position relative to the fault, $y/(TV_R)$. Practically, several studies normalized distance by the square root of drainage area, as drainage area is generally used as a proxy for retreat rate (e.g. Crosby & Whipple, 2006). Knickpoints generated at the same time, along different rivers with different retreat rate, share the same normalized distance relative to the fault. This representation is convenient to assess the spatial extent of an earthquake rupturing several rivers along-strike. Non-normalized river profiles are shown on Figure B1.

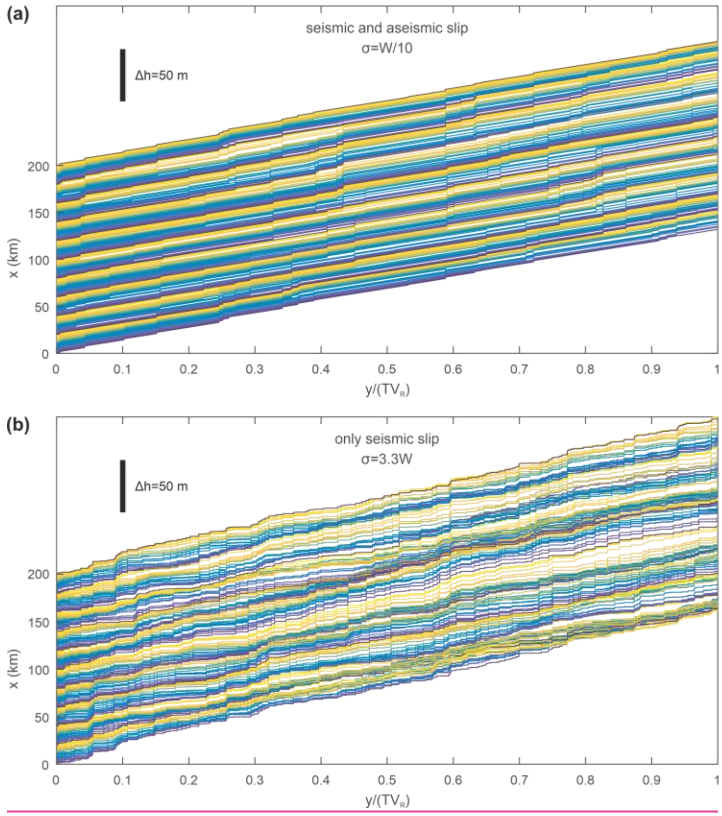

Figure 10. Topography of a set of parallel rivers flowing across-strike the fault. a-b) River profiles of 200 rivers separated by 1 km along the strike of the fault, i.e. the x-direction. River elevation h is given along the same axis, with a scaling factor of 1000. River length y across the strike of fault is normalized by knickpoint migration rate V_R times the duration of the simulation T. Non-normalized river profiles are shown on Figure B1. The colorscale is only present to help figure readability.

Formatted: Font: Times New Roman

6.2 Knickpoint correlation in-between several parallel rivers crossing the fault

This representation is convenient to assess the degree of correlation of the profiles of the successive rivers. Obviously, there is no significant topographic correlation when considering rivers with such a high variability in retreat rates, e.g. 0.001 to 0.1 m.yr^{-1}. We therefore compute the matrix of correlation between each river elevation profile using the river normalized horizontal distance (Fig. B1). River elevation is corrected or “detrended” from its average slope to remove an obvious source of topographic correlation. We then compute the average coefficient of correlation for a given river inter-distance Δx ranging from 0 to 100 km (Fig. 11). The two models, the “only seismic slip” and the “seismic and aseismic slip” models, show a similar pattern, with a significant positive correlation (>0.5) for rivers separated by less than 14 to 23 km (10 to 45 km if accounting for the standard deviation). The maximum distance over which a correlation is significant corresponds to about 35 km, half the maximum co-seismic rupture length of ~70 km along the considered fault. This illustrates that knickpoints should not be correlated for rivers separated by more than this distance, considering the tectonic setting of this model, and fault dimensions. This correlation distance could increase using a wider fault generating larger magnitude earthquake with longer surface rupture. We also find that the correlation is better for the model dominated by aseismic slip and showing less knickpoints (Fig. B1). Positive correlations were obtained using horizontal distance normalized by retreat rate. However, using only catchments with similar retreat rates would also lead to positive and significant correlation even when using non-normalized distance.

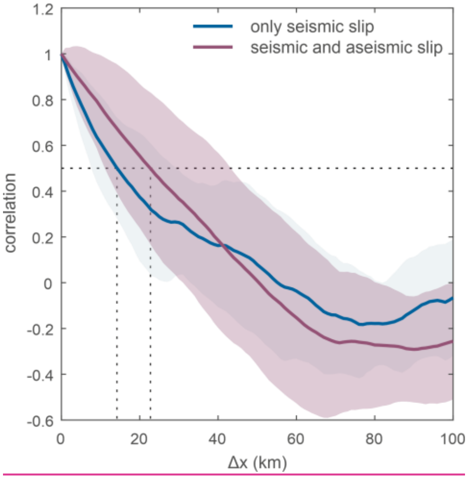

Figure 11. Similarity of river profiles along the strike of the fault. Change of the average coefficient of correlation in-between rivers located along the strike of the fault, with river inter-distance Δx. The double standard deviation is shown by the extent of the shaded area. In blue, the “only seismic slip” model, and in purple the “seismic and aseismic slip” model. The average coefficient of correlation and its standard deviation are measured along the diagonals of the correlation matrix (Fig. B1).

7 Knickpoint detectability

7.1 Knickpoint detectability for the reference model

River profiles are used in many studies to extract co-seismic knickpoints and to assess fault activity and local to regional seismic hazard (e.g. Ewiak et al., 2015; Wei et al., 2015; Sun et al., 2016). It is therefore required to investigate whether modeled knickpoints are statistically detectable. Knickpoint detection often relies on the use of digital elevation models and topographic data (e.g. Neely et al., 2017; Gailleton et al., 2018), which are obtained at a certain scale or resolution. The detectability of each individual knickpoint depends not only on its distance to its adjacent knickpoints, but also on the horizontal resolution and vertical precision of the topographic data and on the roughness of the riverbed. In the following, we consider that a knickpoint is detectable if its height is greater than the vertical precision of topographic data and if its distance to adjacent knickpoints is greater than the horizontal resolution of topographic data.

Resolutions of topographic data available at the global scale (e.g. SRTM or ASTER) are between 10 and 100 m, with precision not better than a few meters. Local to regional topographic datasets obtained from current airborne Lidar or photogrammetric data or derived from aerial or satellite imagery (e.g. Pléiades) display a resolution between 0.5 to about 1-5 m and a typical vertical precision of 10 cm above water. Moreover, in the vertical direction, knickpoint detectability depends also on the inherent bed roughness, mean alluvial deposit thickness and the local distribution of sediment grain size. Sediment grains of dimension greater than 0.1 m are commonly found in rivers located in mountain ranges (e.g. Attal and Lavé, 2006), especially at low drainage areas, and there is often a thin layer of sediment covering the channel bed, potentially hiding bedrock features. If we fully acknowledge the role of river roughness, we here focus on the issue of detectability relative to topographic resolution and precision, for the sake of simplicity, and using knickpoints formed by the “only seismic slip” model.

In terms of vertical precision, a precision of 0.1 m (e.g. Lidar) enables the detection of knickpoints produced by an earthquake as low as magnitude ~4.8 (Fig. 12a). For rivers permanently under water, traditional airborne Lidar using near infrared laser or photogrammetric data cannot measure river bathymetry imposing a detectability level and an uncertainty of knickpoint height of the order of the water depth. Topographic data with a precision of about 1 m would only enable to detect knickpoints for earthquakes of magnitude above 6.8. It results that about 18 % of the knickpoints are detectable using 1 m of precision, while 72 % are detectable with Lidar data and a precision of 0.1 m (Fig. 12b). SRTM or ASTER data have precisions of a few meters, at best, that would only enable the potential detection of earthquakes of magnitude ~8 or more.

In terms of horizontal resolution, we assess knickpoint “detectability” by comparing knickpoint inter-distance with the resolution of topographic data. The distribution of horizontal distance between successive knickpoints (that scales with the distribution of inter-event times) shows that knickpoint inter-distance ranges between less than a millimeter to up to few tens of meters (Fig. 12a). Using a resolution of 10 m, only 7% of the knickpoints can be detected, while a resolution of 1 m increases this percentage to 65 %. Combining horizontal and vertical detectability reduces even more the detectability of knickpoints, as only 2 or 45 % of the knickpoints are detectable using Lidar (1 m of resolution, 0. 1 m of precision) or DEM (10 m of resolution, 1 m of precision) characteristics, respectively.

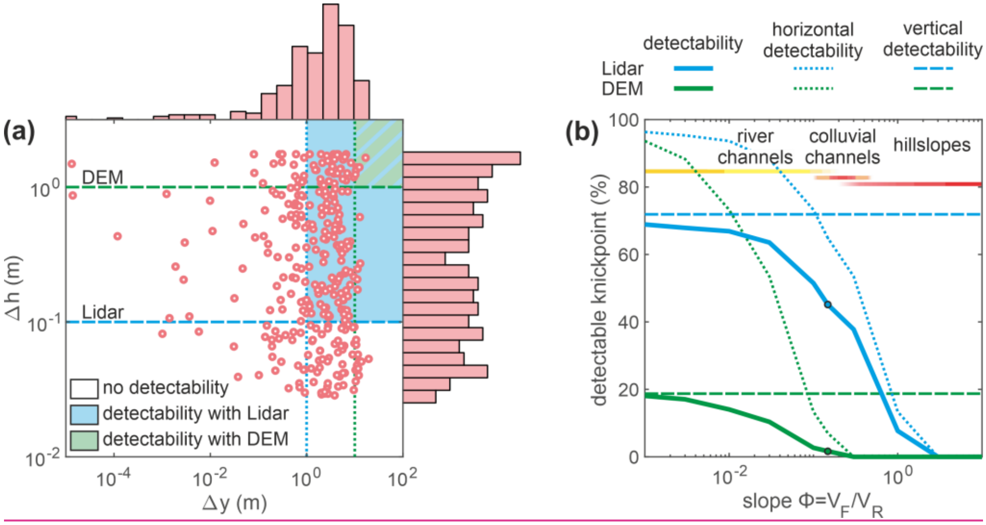

Figure 12. Spatial detectability of individual knickpoints. a) Detectability for the "only seismic slip" model of knickpoints (pink circles) depending on their height Δh and horizontal distance Δy. Limits of resolution (dotted lines) and precision (dashed lines) are indicated for DEM (green) and Lidar data (blue). Domains of DEM or Lidar detectability are indicated by plain green or blue colors, respectively. The marginal distributions are indicated by pink bars. b) Full (bold lines), horizontal (dashed lines) and vertical (dotted lines) knickpoint detectability when varying the ratio φ between knickpoint retreat rate V_R and fault slip rate V_F. φ also represents the river slope and the domains of river channels, colluvial channels and hillslopes are indicated by yellow, orange and red bars. Knickpoint detectability is given as a percentage of the number detected knickpoints over the total number of knickpoints. The blue and green dots represent detectability for the model presented in panel a.

7.2 Knickpoint detectability along rivers, colluvial channels and hillslopes

We now consider the issue of knickpoint detectability for a broader range of model parameters, in particular fault dimensions, fault slip rate and knickpoint retreat rate. Vertical detectability depends only on the range of considered earthquake magnitude and displacement. As the maximum modeled magnitude is directly limited by the dimension of the modeled fault, considering greater knickpoint requires to extend the dimension of the fault and more specifically its width. In our model, horizontal detectability is directly dependent on the river slope, $\varphi = V_F/V_R = 0.15$. Indeed, the horizontal distance between successive knickpoints increases linearly with knickpoint migration velocity V_R, while its decreases linearly with the rate of fault slip V_F that sets the rate of earthquake and knickpoint formation. We here investigate how knickpoint detectability varies with slope φ (Fig. 12b). We consider that river channels have a slope below 0.2, colluvial channels between 0.1 and 0.5 and hillslopes above 0.2, following classical slope-area relationships. In terms of horizontal detectability, rivers with a slope $\varphi < 10^{-2}$ have a good detectability, more than 80 % using Lidar or even DEM resolution. Rivers with $10^{-2} < \varphi < 2.10^{-1}$ have a good horizontal detectability using Lidar data, and a moderate one using DEM (10 to 80 %). Colluvial channels have a moderate horizontal detectability using Lidar data, and a bad one using DEM (< 10 %). Hillslopes with $\varphi > 10^{0}$ have a bad detectability for even with Lidar data. However, the overall detectability of DEM data is below 20 % due to the issue of the vertical detectability, that is low for DEM data. The overall detectability of Lidar data can reach 70% for low values of φ, in the river domain, while it is moderate or even bad for colluvial channels or hillslopes, respectively. This highlights the need for Lidar data to detect in a more systematic manner knickpoints along river or colluvial channels.

8 Discussion

8.1 Model limitations

To approach the problem of co-seismic knickpoint formation and their impact on river profile, we have made several simplifying assumptions. The spatial and temporal distribution of earthquakes, including mainshocks and aftershocks, only follow classical statistical and scaling laws. Fault stress state or friction properties, which are first order controlling factors of earthquake triggering (e.g. Scholz, 1998), are not explicitly accounted for. Earthquake ruptures are assumed to be rectangular, to have dimensions scaling with seismic moment and to display a homogeneous displacement (Leonard, 2010), while natural ruptures display more variable behaviors. The relative contributions of seismic and aseismic processes to fault slip, and their spatial distributions are defined in a relatively ad hoc manner. Moreover, co-seismic displacement follows a block uplift mechanism, which contradicts observations and neglects the elasticity of the lithosphere. Yet, it is to be emphasized that block uplift in near fault conditions for large-magnitude earthquakes corresponds to an asymptotic behavior. A more realistic approach is to compute the surface displacement induced by each earthquake using for instance dislocations embedded into an elastic half-space (e.g. Okada, 1985). This alternative approach would also have the benefit of accounting for the surface displacement of earthquakes that do not rupture the surface. Moreover, surface rupture only occurs along a single fault and does not account for off-fault damage (e.g. Zinke et al., 2014), that could also generate knickpoints, or for more complex rupture geometry (e.g. Romanet et al., 2018). Knickpoint retreat along the river profile was modeled using a constant velocity, which corresponds to an asymptotic behavior of the stream power incision model for small migration distance respective to the square root of river drainage area. If the migration of knickpoints or slope patches are classically modeled using the stream power incision model (Rosenbloom and Anderson, 1994; Whittaker and Boulton, 2012; Royden and Perron, 2013), this approach was recently questioned by experimental (Baynes et al, 2018) and field (Brocard et al., 2016) results suggesting no obvious dependency of the migration rate to river discharge. Mechanistic models of waterfall erosion and retreat offer another more accurate but more complex approach (Scheingross and Lamb, 2017).

8.2 Model and results applicability to normal and strike-slip faults

The developed model, that was applied in this study to a continental thrust fault, can also be directly applied to a normal fault. Indeed, the adopted scaling relationships between earthquake rupture dimensions or displacements and seismic moment (Leonard, 2010) apply to dip-slip earthquakes and therefore to both normal and thrust faults. The main differences are the polarity of motion between hanging and foot wall, and the dipping angle of the fault. This latter difference vanishes in the developed approach as we assume that rupture displacement occurs only in the vertical direction. Under these limitations and simplifications, all the obtained results in this paper can be therefore directly transcribed to normal faults. Because normal faults tend to have a larger dipping angle, close to 60° in average, than thrust faults, the approximation of purely vertical co-seismic displacement is less incorrect for normal faults. Moreover, strike-slip faults or dip-slip faults can also be accounted for by this model, by simply tuning the parameters of the rupture scaling laws, i.e. C_1, C_2, and β. Assuming the depth-distribution of seismicity along different types of faults is identical (a likely incorrect hypothesis), changing the type of fault would not have a major impact on the results presented in this paper.

8.3 Knickpoints and horizontal tectonic displacement

Surface ruptures and displacements were only considered in the vertical direction, clearly simplifying the variability in the orientation of natural surface ruptures. If this paper is focused on the vertical expression of fault along river profiles, future work should account for the influence of horizontal tectonic displacement on river profile (e.g. Miller et al., 2007). Accounting for the dip angle of the fault and the associated horizontal tectonic displacement can have two main effects: 1) move knickpoints in the direction of tectonic motion and increase or decrease the apparent retreat rate of knickpoints, in the case of normal or thrust faults, respectively; and 2) move the position of the fault trace through time, as for instance in the case of a thrust sheet when the hanging wall moves over the footwall. We ignore this latter effect and focus on the influence of tectonic motion on knickpoint retreat rate and on river slope. Accounting for the dipping angle of the fault changes the expression of river slope just upstream of the fault. Indeed, fault slip builds topography in the vertical direction at a rate $V_F \sin(\theta)$ while knickpoints retreat by the cumulative effect of erosion and horizontal tectonic displacement at a rate $V_R \pm V_F \cos(\theta)$. The sign $\pm$ is positive for normal faults but negative for thrust faults, as knickpoints are displaced by tectonics towards the fault trace for this latter. It results that the river slope becomes $\varphi = V_F \sin(\theta) / (V_R + V_F \cos(\theta))$ for normal faults and $\varphi = V_F \sin(\theta) / (V_R + V_F \cos(\theta))$ for thrust faults. For rivers, which generally have slopes lower than about 0.1, the horizontal tectonic displacement $V_F \cos(\theta)$ is likely to be negligible compared to the retreat rate by erosion V_R, and the slope can be approximated by $\varphi \approx V_F \sin(\theta) / V_R$. However, this approximation does not hold anymore for colluvial channels or for hillslopes as the slope becomes closer to 1. Accounting for tectonic displacement obviously changes the threshold of vertical detectability of knickpoints as their height decreases when decreasing the fault dip angle.

8.4 Do mainshocks or aftershocks matter for knickpoints and river profiles?

Aftershocks play a secondary role in the seismicity model considered in this paper. Indeed, for the "only seismic slip" models, aftershocks only represent 18 % of the 442188 earthquakes simulated on the fault. Seismicity is therefore dominated by mainshocks. This is not surprising as about 95% of earthquakes, that follow the Gutenberg-Richter frequency-magnitude distribution, have a magnitude lower than 5 and have in turn a very low probability to generate aftershocks because 1) the aftershock model uses Båth's law with a magnitude difference between any mainshock and their aftershocks, $\Delta Mw = 1.25$, and 2) the minimum magnitude modeled is 3.7. Therefore, aftershocks will only be triggered after intermediate to large magnitude earthquakes, $Mw > 5$, that only represents 5 % of the total number earthquakes. It also results that river profiles in our models are mostly build by mainshocks, and not by aftershocks that only represents 18% of the cumulated uplift. Therefore, developing an aftershock model to include earthquakes and their effects in landscape evolution models represents an additional step in terms of model complexity that is not mandatory. This means that simply accounting for mainshocks by 1) sampling the Gutenberg-Richter distribution to determine earthquake magnitude and 2) randomly sampling their location, already represents a consistent modelling approach towards including earthquakes in landscapes evolution models. Despite that, aftershocks can have significant effects, punctually in time and space, for knickpoint formation, river uplift or even landslide triggering (e.g. Croissant et al., 2019) that justify for some studies the additional complexity of modelling them.

8.5 Knickpoint height distribution as a paleoseismological tool?

Co-seismic knickpoints are common geomorphological markers found in seismic areas (Boulton and Whittaker, 2009; Yanites et al., 2010; Cook et al., 2013). Several studies have offered constraints on fault seismogenic activity from the study of river profile and knickpoint height (Boulton and Whittaker, 2009; Ewiak et al., 2015; Wei et al., 2015; He and Ma, 2015; Sun et al., 2016). Natural distributions of knickpoint height are systematically dominated by large heights, corresponding to earthquake magnitudes greater than 5. For instance, the magnitude of earthquakes deduced from knickpoints extracted along rivers crossing the Atacama Fault System, follows a bell shape distribution favoring large magnitude 5.8-6.9 earthquakes (Ewiak et al., 2015). Because the distributions of knickpoints were found to share similarities with the distribution of ruptures directly along the fault scarp, this rules out the hypothesis of fully eroded co-seismic knickpoints generated by small magnitude earthquakes (Ewiak et al., 2015). This observation, of knickpoints dominated by large earthquakes and the censoring of small magnitude earthquakes, is similar to the results obtained in this paper with the model dominated by aseismic slip at shallow depth (Fig. 3e). Alternative explanations for the apparent lack of small knickpoints or scarp ruptures in most natural datasets (Ewiak et al., 2015; Wei et al., 2015; He and Ma, 2015; Sun et al., 2016) include at least 1) the difficulty to detect the limited displacement induced by earthquakes of magnitude 5 or less and 2) the fault burial mechanism (Finnegan and Balco, 2013; Malatesta and Lamb, 2018) that filters out small co-seismic surface ruptures. In any case, the depth-distribution of earthquakes and of their rupture extent exert fundamental control on the resulting height distribution of co-seismic knickpoint.

In turn, our results suggest that knickpoint datasets, that will become more and more accessible thanks to high-resolution topographic data, can be used to assess fault activity. Obviously, the height of knickpoints provide some form of evidence for the earthquakes that have generated them. A negative exponential distribution of knickpoint height points toward a purely seismic fault, while deviations from this trend can suggest aseismic slip or even a slip deficit at shallow depths. The main limitation is yet the poorly known impact of geomorphological processes on evolution of the shape of knickpoints. Some knickpoints along the Atacama Fault System have a reduced height compare to their initial rupture (Ewiak et al., 2015), while some knickpoints produced during Chi-Chi earthquake in 1999 were higher 10 years later (Yanites et al., 2010). These contrasting cases illustrate some potential, and poorly understood, pitfalls in using knickpoints to infer fault and seismic activity.

8.6 River dynamics: constant uplift or time-variable uplift with earthquakes?

Most numerical efforts attempting at modeling the long-term (>10-100 kyr) topographic building of mountainous or rift settings have used a constant or smoothly varying uplift rate (e.g. Braun and Willett, 2013; Thieulot et al., 2014; Campforts et al., 2017), not including the variability of uplift rate during the seismic cycle. If using a stream power incision model with a linear dependency to slope $n = 1$, this choice is acceptable as the variability of uplift rate and the associated variability of slope patches shaped throughout the seismic cycle can be averaged out. Moreover, knickpoint retreat rate is in this case independent of slope as this model corresponds to a linear kinematic wave equation, (Rosenbloom and Anderson, 1994; Tucker and Whipple, 2002; Whittaker and Boulton, 2012; Royden and Perron, 2013). However, if using a non-linear dependency of erosion rates to slope, with $n \neq 1$, and only considering a long-term averaged uplift rate, and not its variability, is an approximation that becomes more incorrect with the degree of non-linearity of the model. In other words, the erosion rate of a river profile made of co-seismic knickpoints separated by low-slope river sections built during aseismic periods is not equivalent to the erosion rate of a smooth river profile with the same average slope and built under a constant uplift rate. In a non-linear stream power incision model, the retreat rate is sensitive to slope at a power $n - 1$. For $n > 1$, greater slope patches will migrate quicker than lower slope patches, and vice versa for $n < 1$. While a large proportion of the literature considers the linear stream power incision model (or the unit stream power model) as the reference model, the parametrization of the stream power incision and in particular of the slope exponent n is still an open debate, as is its actual applicability to model knickpoint migration (e.g. Lague, 2014). Moreover, the physics of knickpoint or waterfall retreat likely depends on other variables such as knickpoint height (Holland and Pickup, 1976; Hayakawa and Matsukura, 2003; Haviv et al., 2010; Scheingross and Lamb, 2017), sediment supply (Jansen et al., 2011), lithological structure (Lamb and Dietrich, 2009), and lithological strength (Baynes et al., 2018). Even if this debate is clearly out of the scope of this paper, the implication of this study for the understanding of river erosion and dynamics should not be ignored. Indeed, we have shown that even a slight sensitivity of knickpoint retreat rate to knickpoint height leads to large differences in terms of river profile or knickpoint height distribution, by rapidly merging out all small knickpoints into larger ones associated to greater retreat rates (Fig. 7). Moreover, the modelling results of this study show that the frequency-magnitude distribution of earthquakes rupturing a river is uniform for purely seismic faults and follows a bell shape, favoring large magnitude earthquakes, for faults with significant shallow aseismic slip. This result offers a complementary - not an alternative – explanation to the fault-burial mechanism (Malatesta and Lamb, 2018) for the apparent larger proportion of high waterfalls.

8.7 Co-seismic displacements and knickpoints inside landscape evolution models?

Further implications on the impact of considering earthquakes in landscape dynamics can only be casted by using landscape evolution models (LEMs) (Croissant et al., 2017; Davy et al, 2017; Braun and Willett, 2013; Campforts et al., 2017; Egholm et al., 2011). The developed model in this paper can be implemented in most LEMs to investigate river and landscape response to earthquakes and their successions. However, the main foreseen difficulty is the large variability of inter-event times, that put strong constraints on the time stepping strategy. To overcome this difficulty, a minimum earthquake magnitude can be defined as a threshold: earthquakes with lower magnitudes are modelled as continuous fault slip, while earthquakes with greater magnitudes are modelled as discrete uplift events during a specific time step. A second difficulty is the spatial discretization of knickpoints that migrate inside the model domain. Most current LEMs use regular grids to discretize surface topography with a uniform resolution. To be consistent with their boundary conditions, such numerical schemes must adapt their spatial resolution to the typical modeled distance between successive knickpoints that can easily go below 1 m (Fig. 7b). This is problematic as the efficiency of most LEMs scales at best with the number of model nodes~~, at best~~ (e.g. Braun and Willett, 2013). Using too coarse resolutions would smooth out knickpoints and slope variability leading to similar landscape evolution and dynamics as using a constant uplift, even with non-linear slope dependency. Another more adapted strategy is to use irregular grids, for instance based on Delaunay triangulation, to discretize topography in LEMs (e.g. Braun and Sambridge, 1997; Steer et al., 2011). Despite being less commonly used in LEMs, irregular grids enable to properly account for co-seismic knickpoints and variable uplift rates by using fine resolutions close to knickpoints and coarser ones in other model domains. This in turn would lead to tractable model durations. Another benefit of irregular grids is their ability to be deformed in the horizontal directions. This is required to account for the horizontal components of co- or inter-seismic displacement that is systematically ignored in LEMs while being of greater amplitude than vertical displacement in convergent or strike-slip settings (e.g. Cattin and Avouac, 2000). Coupling inter- and co-seismic displacement with LEMs represents a future direction to further investigate the impact of earthquakes and tectonic deformation during the seismic cycle on landscape dynamics. The main remaining limitation is the development of mechanistic models for knickpoint retreat and evolution, a subject that has received recent attention (e.g. Scheingross & Lamb, 2017).

~~6~~9 Conclusions

The accurate modelling of landscape evolution requires accounting for the temporal and spatial variability of surface uplift and displacement. We propose a statistical model of earthquakes, based on the BASS model (Turcotte et al., 2007), to simulate the slope and height distributions generated by earthquakes and aseismic slip at the ~~intersect~~intersection between a thrust fault and a river. The rupture extent and displacement of each earthquake is inferred using classical scaling laws (Leonard, 2010), that can be applied to strike-slip, normal or thrust faults. Slip along the fault plane is partitioned between seismic and aseismic slip using an *ad hoc* spatial distribution of mainshocks along the fault plane. Co-seismic uplift events, with rupture cutting rivers, generate knickpoints that migrate along the river profile following a constant retreat rate.

~~The resulting~~First, the developed model produces ~~co-seismic knickpoints with~~ a uniform ~~height distribution for a fully coupled fault, i.e. with only co-seismic slip. This uniform~~ distribution of ~~knickpoint height and~~ earthquake magnitude cutting the river that is obtained while imposing a Gutenberg-Richter frequency-magnitude distribution of earthquakes along the fault plane ~~respecting the Gutenberg-Richter law with a b value of 1. Partitioning~~. In turn, the produced knickpoint heights follow a negative exponential height distribution. The interevent time distribution between successive knickpoints follows an exponential decay.

Second, partitioning shallow slip between seismic and aseismic slip censors the magnitude range of earthquakes rupturing the surface and cutting the river towards large magnitudes. ~~The interevent time distribution between successive knickpoints follows an exponential decay, independent of the seismogenic rheology of the fault, but the temporal frequency of knickpoint formation increases with fault coupling.~~ Poorly coupled faults, dominated by shallow aseismic slip, generate mostly rare and on average high knickpoints~~. Fully~~ while fully coupled faults~~, dominated by shallow seismic slip,~~ generate frequent knickpoints of moderate height, in average. Assuming no impact of geomorphological processes on the evolution of the shape of knickpoints, an unlikely hypothesis, these differences in the height distribution of knickpoints offer a guide to assess fault coupling and the shallow partitioning of fault slip over longer-time scales than modern seismology.

~~Moreover, the resulting river profiles, in near fault conditions, are also markedly different when produced by fully or poorly coupled faults. Our~~Third, our results demonstrate the influence of earthquakes and of fault properties on river profiles. Using a constant knickpoint retreat rate, our simple model produces river profiles made of a succession of flat sections and knickpoints for fully coupled faults, and straight river profiles with a constant slope and few knickpoints for poorly coupled faults. ~~In turn, fully coupled faults can generate a high spatial density of co-seismic knickpoints along the river profile, requiring high resolutions to distinguish them using digital elevation models. When~~Accounting for a dependency of knickpoint retreat rate to knickpoint height leads to the progressive merging of small knickpoints into larger ones, with a height significantly greater than the vertical offset produced by the largest magnitude earthquakes. Moreover, fault-burial by intermittent sediment cover can alter the surface expression of fault slip and earthquake activity, when the rate of sediment aggradation/degradation is greater than the rate of fault slip.

Fourth, knickpoint detectability, regarding the horizontal resolution and vertical precision of modern topographic datasets such as Lidar or DEMs, directly depends on the river slope that is equal to the ratio between fault slip rate and knickpoint retreat rate. Decreasing the slope increases the horizontal distance between successive knickpoints and enhance knickpoint detectability. On the contrary, the vertical detectability is only limited to the vertical precision of topographic relatively to the topographic offsets produces during earthquakes.

Fifth, when considering several parallel rivers distributed along the strike of the fault, a positive correlation between river profiles is obtained if the rivers are separated by less than half than the maximum rupture length occurring on the fault. This correlation is ~~only ~~obtained ~~when considering river profiles with an~~using a horizontal distance normalized by knickpoint migration rates, or when considering rivers with similar migration rates. The coefficient of correlation becomes significantly positive (>0.5) when the river interdistance is less than about a quarter than the maximum rupture length. For a maximum earthquake magnitude of 7.3, this interdistance corresponds to 14 to 23 km, and does not vary significantly with fault coupling. ~~The~~Last, the developed model offers insights on the building of slopes and knickpoints by fault activity and earthquakes. ~~We have also demonstrated that fault-burial by intermittent sediment cover can alter the surface expression of fault slip and earthquake activity, in particular when the rate of sediment aggradation/degradation is greater than the rate of fault slip. ~~This model could also be implemented in landscape evolution models to better infer the role of tectonics and earthquakes on landscape dynamics. This is pivotal to understand how and why earthquakes build or destroy topography (Parker et al., 2011; Marc et al., 2016), to investigate the feedbacks of erosion on fault dynamics over a seismic cycle (Vernant et al., 2013; Steer et al., 2014) or during orogenesis (Willet et al., 1999; Thieulot et al., 2014), to isolate the feedbacks between river and hillslope dynamics (Valla et al., 2010; Jansen et al., 2011), or to unravel the source-to-sink relationships in seismically active landscapes (Howarth et al., 2012).

Code availability.

A simple Matlab version of the model (Steer and Croissant, 2019) can be accessed through a GitHub and/or a Zenodo repository: https://github.com/philippesteer/RiverFault and https://zenodo.org/record/2654819

~~Appendice A~~

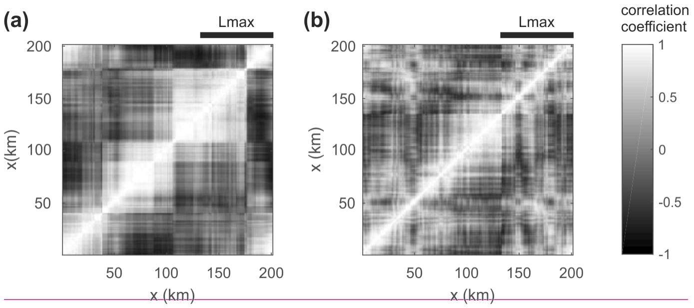

~~Figure A1.~~Appendix A: Constant knickpoint retreat rate and the stream power law

A classical detachment-limited approach to describe the rate of river erosion E is the stream power incision model (Howard and Kerby, 1983; Howard, 1994; Whipple and Tucker, 1999; Lague, 2014) described in Eq. (5):

$$\frac{dh}{dt} = V_F - E = V_F - KA^m \left(\frac{dh}{dy}\right)^n, \tag{5}$$

where h is the elevation of the bedrock bed of the river, t the time, y the distance along the river (i.e. across-strike the fault trace), $S = dh/dy$ the local river slope, A the upstream drainage area, K the erodibility and m and n are two exponents. Considering a linear dependency of erosion rates to slope, with $n = 1$, the stream power incision model is equivalent to a linear kinematic wave equation. Under this condition, it can be demonstrated (Rosenbloom and Anderson, 1994; Tucker and Whipple, 2002; Whittaker and Boulton, 2012; Royden and Perron, 2013) that knickpoints or slope patches along the river migrate upstream at a rate determined by Eq. (6):

$$V_R = \frac{dy}{dt} = KA^m. \tag{6}$$

Moreover, recent empirical results suggest that using $n = 1$ and $m = 0.5$ is suited to describe knickpoint migration (Lague, 2014). If the total migration distance is small compared to the entire river length, from its source to the modeled frontal thrust fault, the migration velocity V_R can be approximated as a constant. This condition holds only if $KT \ll 1$, considering that river length generally scales with about the square root of drainage area (Hack, 1957). The horizontal knickpoint retreat rate $V_R = 0.1$ m.yr^{-1} can therefore be obtained for an infinity of couples of the A and K parameters, following the relationship $V_R = KA^m$, that yet must at least satisfy the condition $KT \ll 1$ (Fig. A1). Other conditions exist, including the domain of validity in the A space of the stream power incision model or that the slope generated for a given value of A makes sense in terms of river steepness. However, they are not further considered as the scope of this paper is to develop a general quantitative framework to investigate slope and topographic building by a fault.

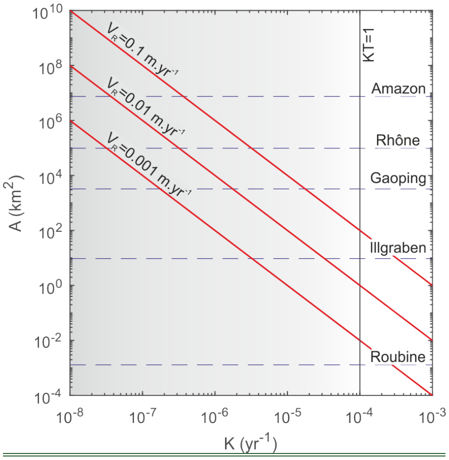

Figure A1. Range of possible couples of parameters of river drainage area A and erodibility K for different values of retreat rate V_R (red lines). The vertical black line indicates the uppermost value of K, as $KT \ll 1$. The range of acceptable values of K is indicated by a gradient from white (non-acceptable) to grey (acceptable). The drainage area A of some iconic catchments are indicated with dashed blue lines and include the Amazon (south America), Rhône (Europe), Gaoping (Taiwan), Illgraben (Switzerland) and Roubine (France) rivers.

Appendix B: Parallel rivers topographic correlation

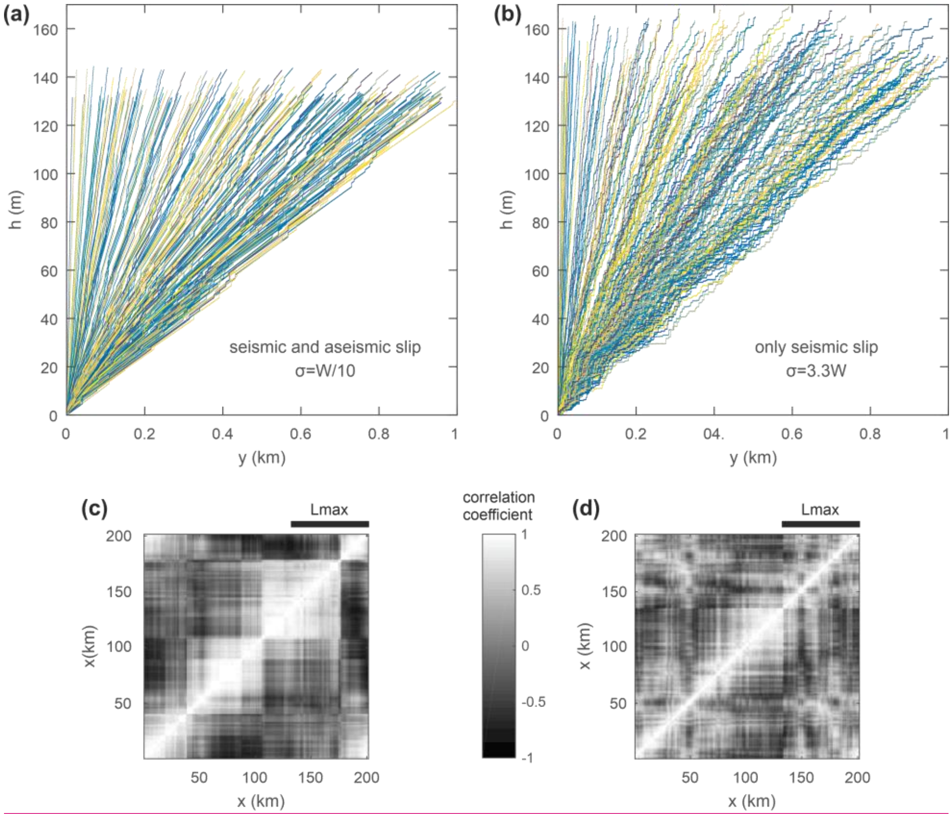

Figure B1. Correlation matrixes showing the coefficient of correlation in-between the 200 river profiles shown in Figure 8 a and b, respectively. The correlation is performed on detrended river profiles. ~~Panels~~Panel a shows results of the “only seismic slip” model~~ with $\sigma = W/10$~~, while ~~panels~~panel b shows results of the ~~reference~~“seismic and aseismic slip” model~~ with $\sigma = 3.3W$~~.

Appendix C: Table of variable definition and notation

Variable	Definition
M_0	Earthquake moment magnitude
Mw	Earthquake magnitude
$N(\geq Mw)$	Cumulative number of earthquakes of magnitude greater than Mw
$N(Mw)$.	Incremental number of earthquakes of magnitude Mw
a	Gutenberg-Richter earthquake productivity
b	Gutenberg-Richter b-value
R	Rate of mainshock
ΔMw	Magnitude difference of Båth's law
p	Exponent of the temporal Omori's law
c	Offset of temporal Omori's law
q	Exponent of the spatial Omori's law
d	Offset of the spatial Omori's law
L_{rup}	Earthquake rupture length
W_{rup}	Earthquake rupture width
C_1	Earthquake scaling law constant
C_2	Earthquake scaling law constant
β	Earthquake scaling law exponent
μ	Elastic shear modulus
L	Fault length
W	Fault width
D	Earthquake rupture mean displacement
θ	Fault dip angle
V_F	Average fault slip rate
V_S	Seismic fault slip rate
V_A	Aseismic fault slip rate
χ	Average degree of seismic coupling
σ	Variance of the normal depth distribution of mainshocks
T	Simulation duration
t	Simulation time
x	Along-fault coordinate
y	Along-river coordinate

h	The bedrock riverbed elevation
hs	Sediment cover thickness
V_R	Knickpoint retreat rate
r	Retreat rate constant
Δh	Knickpoint height
Δh_0	Reference knickpoint height
q	Retreat rate exponent
K	Erodibility
A	Drainage area
m, n	Exponents of the stream power law
φ	Average river slope just upstream the fault

Table C1. Table of variable definition and notation.

Author contributions

PS wrote the paper and designed this study. PS and TC developed the accompanying numerical model. EB and DL motivated the paper through insightful discussions around river profiles and co-seismic knickpoints. All authors checked and revised the text and the figures of the paper, contributed to ideas developed in this study, and discussed the implications for geomorphology and river profile analysis.

Competing interests.

The authors declare that they have no conflict of interest.

Acknowledgments.

We thank Louise Jeandet, Maxime Mouyen, Michaël Pons, Rodolphe Cattin and Philippe Davy for their helpful comments and for discussions about this work. We also thank Wolfgang Schwanghart, Robert Sare, George Hilley, an anonymous reviewer as well as the editor for their many positive and constructive comments that have contributed to enhance the quality of this manuscript. We acknowledge support by Université Rennes 1, by the Boost'ERC project funded by Région Bretagne, by the French-Taiwanese International Laboratory D3E~~ and~~, by the EROQUAKE project funded by the Agence Nationale de la Recherche (ANR-14-CE33-0005~~).~~) and by by a European Research Council (ERC) Starting Grant (803721) to Philippe Steer.

References

Aki, K.: A probabilistic synthesis of precursory phenomena, in: Earthquake prediction: an international review, edited by: Simpson, D. W. and Richards, P. G., AGU, Washington, D.C., USA, 566-574, vol. 4, 1981.

Antón, L., Mather, A. E., Stokes, M., Munoz-Martin, A. and De Vicente, G.: Exceptional river gorge formation from unexceptional floods, Nature communications, 6, 7963, 2015.

Arrowsmith, J. R., Pollard, D. D. and Rhodes, D. D.: Hillslope development in areas of active tectonics, Journal of Geophysical Research: Solid Earth, 101(B3), 6255-6275, 1996.

Arrowsmith, J. R., Rhodes, D. D. and Pollard, D. D.: Morphologic dating of scarps formed by repeated slip events along the San Andreas Fault, Carrizo Plain, California, Journal of Geophysical Research: Solid Earth, 103(B5), 10141-10160, 1998.

Attal, M. and Lavé, J.: Changes of bedload characteristics along the Marsyandi River (central Nepal): Implications for understanding hillslope sediment supply, sediment load evolution along fluvial networks, and denudation in active orogenic belts, in: Tectonics, climate, and landscape evolution, 398, 143, 2006.

Avouac, J. P.: Analysis of scarp profiles: evaluation of errors in morphologic dating, Journal of Geophysical Research: Solid Earth, 98(B4), 6745-6754, 1993.

Avouac, J. P.: From geodetic imaging of seismic and aseismic fault slip to dynamic modeling of the seismic cycle, Annual Review of Earth and Planetary Sciences, 43, 233-271, 2015

Baynes, E. R., Attal, M., Niedermann, S., Kirstein, L. A., Dugmore, A. J. and Naylor, M.: Erosion during extreme flood events dominates Holocene canyon evolution in northeast Iceland, Proceedings of the National Academy of Sciences, 201415443, 2015.

Baynes, E. R., Lague, D., Attal, M., Gangloff, A., Kirstein, L. A. and Dugmore, A. J.: River self-organisation inhibits discharge control on waterfall migration, Scientific reports, 8(1), 2444, 2018.

Berlin, M. M. and Anderson, R. S.: Modeling of knickpoint retreat on the Roan Plateau, western Colorado. Journal of Geophysical Research: Earth Surface, 112(F3), 2007.

Bishop, P., Hoey, T. B., Jansen, J. D. and Artza, I. L.: Knickpoint recession rate and catchment area: the case of uplifted rivers in Eastern Scotland, Earth Surface Processes and Landforms, 30(6), 767-778, 2005.

Boncio, P., Liberi, F., Caldarella, M. and Nurminen, F. C.: Width of surface rupture zone for thrust earthquakes: implications for earthquake fault zoning, Natural Hazards and Earth System Sciences, 18(1), 241-256, 2018.

Boulton, S. J. and Whittaker, A. C.: Quantifying the slip rates, spatial distribution and evolution of active normal faults from geomorphic analysis: Field examples from an oblique-extensional graben, southern Turkey, Geomorphology, 104(3-4), 299-316, 2009.

Braun, J. and Sambridge, M.: Modelling landscape evolution on geological time scales: a new method based on irregular spatial discretization. Basin Research, 9(1), 27-52, 1997

Braun, J. and Willett, S. D.: A very efficient O (n), implicit and parallel method to solve the stream power equation governing fluvial incision and landscape evolution, Geomorphology, 180, 170-179, 2013.

Braun, J.: The many surface expressions of mantle dynamics. Nature Geoscience, 3(12), 825, 2010.

Brocard, G. Y., Willenbring, J. K., Miller, T. E. and Scatena, F. N.: Relict landscape resistance to dissection by upstream migrating knickpoints, Journal of Geophysical Research: Earth Surface, 121, 1182–1203, 2016.

Campforts, B., Schwanghart, W. and Govers, G.: Accurate simulation of transient landscape evolution by eliminating numerical diffusion: the TTLEM 1.0 model, Earth Surface Dynamics, 5, 47-66, 2017.

Carretier, S. and Lucazeau, F.: How does alluvial sedimentation at range fronts modify the erosional dynamics of mountain catchments?, Basin research, 17(3), 361-381, 2005.

Castelltort, S., Goren, L., Willett, S. D., Champagnac, J. D., Herman, F. and Braun, J.: River drainage patterns in the New Zealand Alps primarily controlled by plate tectonic strain. Nature Geoscience, 5(10), 744, 2012.

Cattin, R. and Avouac, J. P.: Modeling mountain building and the seismic cycle in the Himalaya of Nepal, Journal of Geophysical Research: Solid Earth, 105(B6), 13389-13407, 2000.

Chen, Y. G., Chen, W. S., Lee, J. C., Lee, Y. H., Lee, C. T., Chang, H. C. and Lo, C. H.: Surface rupture of 1999 Chi-Chi earthquake yields insights on active tectonics of central Taiwan, Bulletin of the Seismological Society of America, 91(5), 977-985, 2001.

Cook, K. L., Turowski, J. M. and Hovius, N.:A demonstration of the importance of bedload transport for fluvial bedrock erosion and knickpoint propagation, Earth Surface Processes and Landforms, 38(7), 683-695, 2013.

Croissant, T., Lague, D., Steer, P. and Davy, P.: Rapid post-seismic landslide evacuation boosted by dynamic river width, Nature Geoscience, 10(9), 680, 2017.

Croissant, T., Steer, P., Lague, D., Davy, P., Jeandet, L., and Hilton, R. G.: Seismic cycles, earthquakes, landslides and sediment fluxes: Linking tectonics to surface processes using a reduced-complexity model, Geomorphology, 339, 87-103 2019.

Crosby, B. T. and Whipple, K. X.: Knickpoint initiation and distribution within fluvial networks: 236 waterfalls in the Waipaoa River, North Island, New Zealand, Geomorphology, 82(1-2), 16-38, 2006.

Davy, P., Croissant, T. and Lague, D.: A precipiton method to calculate river hydrodynamics, with applications to flood prediction, landscape evolution models, and braiding instabilities~~.~~, Journal of Geophysical Research: Earth Surface, 122(8), 1491-1512, 2017.

Dorsey, R. J. and Roering, J. J.: Quaternary landscape evolution in the San Jacinto fault zone, Peninsular Ranges of Southern California: Transient response to strike-slip fault initiation, Geomorphology, 73(1-2), 16-32, 2006.

Egholm, D. L., Knudsen, M. F., Clark, C. D. and Lesemann, J. E.: Modeling the flow of glaciers in steep terrains: The integrated second-order shallow ice approximation (iSOSIA), Journal of Geophysical Research: Earth Surface, 116(F2), 2011.

Ewiak, O., Victor, P. and Oncken, O.: Investigating multiple fault rupture at the Salar del Carmen segment of the Atacama Fault System (northern Chile): Fault scarp morphology and knickpoint analysis, Tectonics, 34(2), 187-212, 2015.

Finnegan, N. J. and Balco, G.: Sediment supply, base level, braiding, and bedrock river terrace formation: Arroyo Seco, California, USA, GSA Bulletin, 125(7-8), 1114-1124, 2013.

~~Flint, J. J.: Stream gradient as a function of order, magnitude, and discharge, Water Resources Research, 10(5), 969-973, 1974.~~

Gailleton, B., Mudd, S. M., Clubb, F. J., Peifer, D. and Hurst, M. D.: A segmentation approach for the reproducible extraction and quantification of knickpoints from river long profiles, Earth Surface Dynamics Discussion, 2018.

Gilbert, G.K.: Niagara Falls and their history, in: National Geographic Society, The Physiography of the United States, The American Book Co., New York, USA, 203-236, 1896.

Gilbert, G. K.: Rate of recession of Niagara Falls, in: U.S. Geological Survey Bulletin, 306, 1907.

Goren, L., Castelltort, S. and Klinger, Y.: Modes and rates of horizontal deformation from rotated river basins: Application to the Dead Sea fault system in Lebanon, Geology, 43(9), 843-846, 2015.

Gutenberg, B. and Richter, C. F.: Frequency of earthquakes in California. Bulletin of the Seismological Society of America, 34(4), 185-188, 1944.

Hack, J. T.: Studies of longitudinal stream profiles in Virginia and Maryland, U.S. Geological Survey Bulletin, 294, 1957.

Haviv, I., Enzel, Y., Whipple, K. X., Zilberman, E., Matmon, A., Stone, J. and Fifield, K. L.: Evolution of vertical knickpoints (waterfalls) with resistant caprock: Insights from numerical modelling, Journal of Geophysical Research: Earth Surface, 115(F3), 2010.

Hayakawa, Y. and Matsukura, Y.: Recession rates of waterfalls in Boso Peninsula, Japan, and a predictive equation, Earth Surface Processes and Landforms, 28(6), 675-684, 2003.

He, Z. and Ma, B.: Holocene paleoearthquakes of the Daqingshan fault detected from knickpoint identification and alluvial soil profile, Journal of Asian Earth Sciences, 98, 261-271, 2015.

Helmstetter, A. and Sornette, D.: Foreshocks explained by cascades of triggered seismicity, Journal of Geophysical Research: Solid Earth, 108(B10), 2003

Herman, F. and Braun, J.: Evolution of the glacial landscape of the Southern Alps of New Zealand: Insights from a glacial erosion model, Journal of Geophysical Research: Earth Surface, 113(F2), 2008

Holland, W. N. and Pickup, G., Flume study of knickpoint development in stratified sediment, Geological Society of America Bulletin, 87(1), 76-82, 1976.

Hovius, N., Meunier, P., Lin, C. W., Chen, H., Chen, Y. G., Dadson, S., Ming-Jame, H. and Lines, M.: Prolonged seismically induced erosion and the mass balance of a large earthquake. Earth and Planetary Science Letters, 304(3-4), 347-355, 2011.

Howard, A. D. and Kerby, G.: Channel changes in badlands. Geological Society of America Bulletin, 94(6), 739-752, 1983.

Howard, A. D., Dietrich, W. E. and Seidl, M. A.: Modeling fluvial erosion on regional to continental scales, Journal of Geophysical Research: Solid Earth, 99(B7), 13971-13986, 1994.

Howarth, J. D., Fitzsimons, S. J., Norris, R. J. and Jacobsen, G. E.: Lake sediments record cycles of sediment flux driven by large earthquakes on the Alpine fault, New Zealand, Geology, 40(12), 1091-1094, 2012.

Jansen, J. D., Fabel, D., Bishop, P., Xu, S., Schnabel, C. and Codilean, A. T.: Does decreasing paraglacial sediment supply slow knickpoint retreat?, Geology, 39(6), 543-546, 2011.

Jolivet, R., Simons, M., Agram, P. S., Duputel, Z. and Shen, Z. K.: Aseismic slip and seismogenic coupling along the central San Andreas Fault, Geophysical Research Letters, 42(2), 297-306, 2015.

Kanamori, H.: The energy release in great earthquakes, Journal of geophysical research, 82(20), 2981-2987, 1977.

Keefer, D. K.: The importance of earthquake-induced landslides to long-term slope erosion and slope-failure hazards in seismically active regions, in: Geomorphology and Natural Hazards, 265-284, 1994.

King, G.: The accommodation of large strains in the upper lithosphere of the earth and other solids by self-similar fault systems: the geometrical origin of b-value, Pure and Applied Geophysics, 121(5-6), 761-815, 1983.

Lague, D.: The stream power river incision model: evidence, theory and beyond, Earth Surface Processes and Landforms, 39(1), 38-61, 2014.

Lamb, M. P. and Dietrich, W. E.: The persistence of waterfalls in fractured rock, Geological Society of America Bulletin, 121(7-8), 1123-1134, 2009.

Leonard, M.: Earthquake fault scaling: Self-consistent relating of rupture length, width, average displacement, and moment release, Bulletin of the Seismological Society of America, 100(5A), 1971-1988, 2010.

Loget, N., Davy, P. and Van den Driessche, J.: Mesoscale fluvial erosion parameters deduced from modeling the Mediterranean sea level drop during the Messinian (late Miocene), Journal of Geophysical Research: Earth Surface, 111(F3), 2006.

Loget, N. and Van Den Driessche, J.: Wave train model for knickpoint migration, Geomorphology, 106(3-4), 376-382, 2009.

Malatesta, L. C. and Lamb, M. P.: Formation of waterfalls by intermittent burial of active faults, GSA Bulletin, 130(3-4), 522-536, 2018.

Marc, O., Hovius, N. and Meunier, P.: The mass balance of earthquakes and earthquake sequences, Geophysical Research Letters, 43(8), 3708-3716, 2016.

Marone, C. and Scholz, C. H.: The depth of seismic faulting and the upper transition from stable to unstable slip regimes, Geophysical Research Letters, 15(6), 621-624, 1988.

McKean, J. A., Dietrich, W. E., Finkel, R. C., Southon, J. R. and Caffee, M. W~~. :~~.: Quantification of soil production and downslope creep rates from cosmogenic 10Be accumulations on a hillslope profile, Geology, 21(4), 343-346, 1993.

Miller, S. R., Slingerland, R. L. and Kirby, E.: Characteristics of steady state fluvial topography above fault-bend folds, Journal of Geophysical Research: Earth Surface, 112(F4), 2007.

Nash, D. B.: Morphologic dating of degraded normal fault scarps, The Journal of Geology, 88(3), 353-360, 1980.

Neely, A. B., Bookhagen, B. and Burbank, D. W.: An automated knickzone selection algorithm (KZ-Picker) to analyze transient landscapes: Calibration and validation, Journal of Geophysical Research: Earth Surface, 122(6), 1236-1261, 2017.

Ogata, Y.: Statistical models for earthquake occurrences and residual analysis for point processes, Journal of the American Statistical association, 83(401), 9-27, 1988.

Okada, Y.: Surface deformation due to shear and tensile faults in a half-space, Bulletin of the seismological society of America, 75(4), 1135-1154, 1985.

Parker, R.S.: Experimental study of drainage basin evolution and its hydrologic implications, PhD dissertation, Colorado State University, Fort Collins, 1977.

Parker, R. N., Densmore, A. L., Rosser, N. J., De Michele, M., Li, Y., Huang, R., Whadcoat, S. and Petley, D. N.: Mass wasting triggered by the 2008 Wenchuan earthquake is greater than orogenic growth, Nature Geoscience, 4(7), 449, 2011

Peng, Z. and Gomberg, J.: An integrated perspective of the continuum between earthquakes and slow-slip phenomena. Nature Geoscience, 3(9), 599, 2010.

Quigley, M. C., Cupper, M. L. and Sandiford, M.: Quaternary faults of south-central Australia: palaeoseismicity, slip rates and origin, Australian Journal of Earth Sciences, 53(2), 285-301, 2006.

Roering, J. J., Kirchner, J. W. and Dietrich, W. E.: Evidence for nonlinear, diffusive sediment transport on hillslopes and implications for landscape morphology, Water Resources Research, 35(3), 853-870, 1999.

Romanet, P., Bhat, H. S., Jolivet, R. and Madariaga, R.: Fast and slow slip events emerge due to fault geometrical complexity, Geophysical Research Letters, 45(10), 4809-4819, 2018.

Rosenbloom, N. A. and Anderson, R. S.: Hillslope and channel evolution in a marine terraced landscape, Santa Cruz, California, Journal of Geophysical Research: Solid Earth, 99(B7), 14013-14029, 1994.

Royden, L. and Perron, J. T., Solutions of the stream power equation and application to the evolution of river longitudinal profiles, Journal of Geophysical Research: Earth Surface, 118(2), 497-518, 2013.

Scheingross, J. S. and Lamb, M. P.: A mechanistic model of waterfall plunge pool erosion into bedrock, Journal of Geophysical Research: Earth Surface, 122(11), 2079-2104, 2017.

Schmittbuhl, J., Karabulut, H., Lengliné, O. and Bouchon, M.: Seismicity distribution and locking depth along the Main Marmara Fault, Turkey, Geochemistry, Geophysics, Geosystems, 17(3), 954-965, 2015.

Scholz, C. H.: Earthquakes and friction laws, Nature, 391(6662), 37, 1998.

Schumm, S. A., Mosley, M. P. and Weaver W.E.: Experimental Fluvial Geomorphology, in: John Wiley and Sons, New York, 413, 1987.

Shcherbakov, R. and Turcotte, D. L.: A modified form of Bath's law, Bulletin of the Seismological Society of America, 94(5), 1968-1975, 2004.

Shcherbakov, R., Turcotte, D. L. and Rundle, J. B.: A generalized Omori's law for earthquake aftershock decay, Geophysical research letters, 31(11), 2004.

Sibson, R. H.: Fault zone models, heat flow, and the depth distribution of earthquakes in the continental crust of the United States, Bulletin of the Seismological Society of America, 72(1), 151-163, 1982.

Steer, P. and Croissant, T.: philippesteer/RiverFault: Initial version, doi:10.5281/zenodo.2654819, 2019.

Steer, P., Cattin, R., Lavé, J. and Godard, V.: Surface Lagrangian Remeshing: A new tool for studying long term evolution of continental lithosphere from 2D numerical modelling. Computers and geosciences, 37(8), 1067-1074, 2011.

Steer, P., Simoes, M., Cattin, R. and Shyu, J. B. H.: Erosion influences the seismicity of active thrust faults, Nature communications, 5, 5564, 2014.

Stock, J. D. and Montgomery, D. R.: Geologic constraints on bedrock river incision using the stream power law, Journal of Geophysical Research: Solid Earth, 104(B3), 4983-4993, 1999.

Sun, C., Wan, T., Xie, X., Shen, X. and Liang, K.: Knickpoint series of gullies along the Luoyunshan Piedmont and its relation with fault activity since late Pleistocene, Geomorphology, 268, 266-274, 2016.

Thieulot, C., Steer, P. and Huismans, R. S.: Three-dimensional numerical simulations of crustal systems undergoing orogeny and subjected to surface processes, Geochemistry, Geophysics, Geosystems, 15(12), 4936-4957, 2014.

Tucker, G. E. and Bradley, D. N.: Trouble with diffusion: Reassessing hillslope erosion laws with a particle-based model, Journal of Geophysical Research: Earth Surface, 115(F1), 2010.

Tucker, G. E. and Whipple, K. X.: Topographic outcomes predicted by stream erosion models: Sensitivity analysis and intermodel comparison. Journal of Geophysical Research: Solid Earth, 107(B9), 2002.

Turcotte, D. L., Holliday, J. R. and Rundle, J. B.: BASS, an alternative to ETAS, Geophysical research letters, 34(12), 2007.

van der Beek, P., Pulford, A., & Braun, J.: Cenozoic landscape development in the Blue Mountains (SE Australia): lithological and tectonic controls on rifted margin morphology, The Journal of Geology, 109(1), 35-56, 2001.

Van Heijst, M. W. I. M. and Postma, G.: Fluvial response to sea-level changes: a quantitative analogue, experimental approach, Basin Research, 13(3), 269-292, 2001.

Valla, P. G., Van Der Beek, P. A. and Lague, D.: Fluvial incision into bedrock: Insights from morphometric analysis and numerical modeling of gorges incising glacial hanging valleys (Western Alps, France), Journal of Geophysical Research: Earth Surface, 115(F2), 2010.

Vernant, P., Hivert, F., Chery, J., Steer, P., Cattin, R. and Rigo, A.: Erosion-induced isostatic rebound triggers extension in low convergent mountain ranges, Geology, 41(4), 467-470, 2013.

Watts, A. B.: Isostasy and Flexure of the Lithosphere, in: Cambridge University Press, 2001.

Wei, Z., Bi, L., Xu, Y. and He, H.: Evaluating knickpoint recession along an active fault for paleoseismological analysis: The Huoshan Piedmont, Eastern China, Geomorphology, 235, 63-76, 2015.

Wells, D. L. and Coppersmith, K. J.: New empirical relationships among magnitude, rupture length, rupture width, rupture area, and surface displacement, Bulletin of the seismological Society of America, 84(4), 974-1002, 1994.

Whipple, K. X. and Tucker, G. E.: Dynamics of the stream-power river incision model: Implications for height limits of mountain ranges, landscape response timescales, and research needs, Journal of Geophysical Research: Solid Earth, 104(B8), 17661-17674, 1999.

Whipple, K. X.: The influence of climate on the tectonic evolution of mountain belts, Nature Geoscience, 2(2), 97, 2009.

Whittaker, A. C. and Boulton, S. J.: Tectonic and climatic controls on knickpoint retreat rates and landscape response times, Journal of Geophysical Research: Earth Surface, 117(F2), 2012.

Willett, S. D.: Orogeny and orography: The effects of erosion on the structure of mountain belts, Journal of Geophysical Research: Solid Earth, 104(B12), 28957-28981, 1999.

Yanites, B. J., Tucker, G. E., Mueller, K. J., Chen, Y. G., Wilcox, T., Huang, S. Y. and Shi, K. W.: Incision and channel morphology across active structures along the Peikang River, central Taiwan: Implications for the importance of channel width, GSA Bulletin, 122(7-8), 1192-1208, 2010.

Yildirim, C., Schildgen, T. F., Echtler, H., Melnick, D. and Strecker, M. R.: Late Neogene and active orogenic uplift in the Central Pontides associated with the North Anatolian Fault: Implications for the northern margin of the Central Anatolian Plateau, Turkey, Tectonics, 30(5), 2011.

Zinke, R., Hollingsworth, J. and Dolan, J. F.: Surface slip and off-fault deformation patterns in the 2013 Mw 7.7 Balochistan, Pakistan earthquake: Implications for controls on the distribution of near-surface coseismic slip, Geochemistry, Geophysics, Geosystems, 15(12), 5034-5050, 2014.

Formatted: Font: Times New Roman, Not Bold, English (United Kingdom)